Slip effects in polymer thin films

2010 J. Phys.: Condens. Matter 22 033102

(http://iopscience.iop.org/0953-8984/22/3/033102)

IOP Publishing Journal of Physics: Condensed Matter

J. Phys.: Condens. Matter **22** (2010) 033102 (21pp) doi:10.1088/0953-8984/22/3/033102

TOPICAL REVIEW

Slip effects in polymer thin films

O Bäumchen and K Jacobs

Department of Experimental Physics, Saarland University, D-66041 Saarbrücken, Germany

E-mail: k.jacobs@physik.uni-saarland.de

Received 10 September 2009, in final form 11 November 2009
Published 16 December 2009
Online at stacks.iop.org/JPhysCM/22/033102

Abstract

Probing the fluid dynamics of thin films is an excellent tool for studying the solid/liquid boundary condition. There is no need for external stimulation or pumping of the liquid, due to the fact that the dewetting process, an internal mechanism, acts as a driving force for liquid flow. Viscous dissipation, within the liquid, and slippage balance interfacial forces. Thus, friction at the solid/liquid interface plays a key role towards the flow dynamics of the liquid. Probing the temporal and spatial evolution of growing holes or retracting straight fronts gives, in combination with theoretical models, information on the liquid flow field and, especially, the boundary condition at the interface. We review the basic models and experimental results obtained during the last several years with exclusive regard to polymers as ideal model liquids for fluid flow. Moreover, concepts that aim to explain slippage on the molecular scale are summarized and discussed.

(Some figures in this article are in colour only in the electronic version)

Contents

1. Introduction

Understanding liquid flow in confined geometries plays a huge role in the field of micro- and nanofluidics [1]. Nowadays, microfluidic or 'lab-on-chip' devices are utilized in a wide range of applications. Pure chemical reactions, as well as biological analysis performed on such a microfluidic chip, allow high performance with only small amounts of chemicals being needed. Thus, analogies to electronic large-scale integrated circuits are evident. Thorsen *et al* fabricated a microfluidic chip with a high density of micromechanical valves and hundreds of individually addressable chambers [2]. Recent developments tend to avoid huge external features such as pumps to control the flow by designing analogs to capacitors, resistors or diodes that are capable of controlling currents in electronic circuits [3].

By reducing the spatial dimensions of liquid volume in confined geometries, slippage can have a huge impact on flow dynamics. Specifically, the problem of driving small amounts of liquid volume through narrow channels has drawn the attention of many researchers on slip effects at the solid/liquid interface. The aim is to reduce the pressure that is needed to induce and to maintain the flow. Hence, the liquid throughput is increased and, importantly in the case of

polydisperse liquids or mixtures, a low dispersity according to lower velocity gradients perpendicular to the flow direction is generated. Confined geometries are realized in various types of experiments: the physics and chemistry of the imbibition of liquids by porous media is of fundamental interest and enormous technological relevance [4]. Channel-like three-dimensional structures can be used to artificially model the situation of fluids in confinement. Moreover, the small gap between a colloidal probe and a surface filled with a liquid (e.g. realized in surface force apparatus or colloidal probe atomic force microscopy experiments) is a common tool to study liquid flow properties. Besides the aforementioned experimental systems, knowledge in preparation of thin polymer films has been extensively gained due to its enormous relevance in coating and semiconductor processing technology. Such a homogeneous nanometric polymer film supported by a very smooth substrate, as for example a piece of a silicon (Si) wafer, exhibits two relevant interfaces, the liquid/air and the substrate/liquid interface. Si wafers are often used due to their very low roughness and controllable oxide layer thickness. Yet, also highly viscous and elastically deformable supports, such as e.g. polydimethylsiloxane (PDMS) layers, are versatile substrates.

The stability of a thin film is governed by the effective interface potential ϕ as a function of film thickness h. In the case of dielectric systems, $\phi(h)$ is composed of an attractive van der Waals part and a repulsive part [5–8]. For the description of the van der Waals forces of a composite substrate, the layer thicknesses and their respective polarization properties have to be taken into account [9]. Therefore, three major situations of a thin liquid film have to be distinguished: *stable*, *unstable* and *metastable* films. As illustrated in figure 1 by the typical curves of $\phi(h)$, a *stable* liquid film is obtained if the effective interface potential is positive and monotonically decaying (cf curve (1) in figure 1). The equilibrium film thickness h_{eq} is infinite and the liquid perfectly wets the substrate. In the case of a global minimum of $\phi(h)$, curves (2) and (3) in figure 1, the system can minimize its energy and a finite value for h_{eq} results. The *metastable* situation is further characterized by a potential barrier that the system has to overcome to reduce its potential energy (cf curve (2) in figure 1). Curves (3) and (4) characterize *unstable* conditions, since every slight fluctuation in film height will drive the system towards the global minimum. The wettability of the substrate by the liquid is correlated to the depth of the minimum at $\phi(h_{\mathrm{eq}})$. The deeper the global minimum of ϕ, the larger the equilibrium contact angle of the liquid on the surface is. A nearly 180° situation is depicted by curve (4) in figure 1.

For a 100 nm polystyrene (PS) film on a hydrophobized Si wafer with a native oxide layer, dewetting starts after heating the sample above the glass transition temperature of the polymer. Holes nucleate according to thermal activation or nucleation spots (dust particles, inhomogeneities of the substrate or of the polymer film) and grow with time, cf figure 2. The subsequent stages of dewetting are characterized by the formation of liquid ridges through the coalescence of growing holes and traveling fronts. Very thin films in the range of several nanometers may become unstable and can

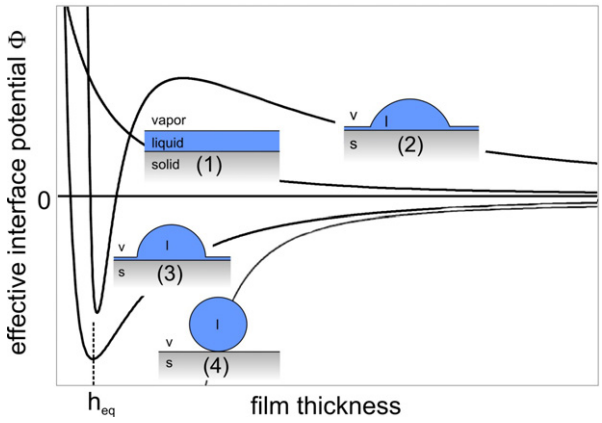

Figure 1. Different shapes of the effective interface potential $\phi(h)$ associated with different wetting conditions. Curve (1) characterizes a *stable* liquid film. Curve (2) represents a *metastable*, curve (3) and (4) an *unstable* situation.

dewet according to thermally induced capillary modes, which are amplified by forces contributing to the effective interface potential. This phenomenon is characterized by the occurrence of a preferred wavelength and is called *spinodal dewetting*. To study thin film flow with regard to the influence of slippage, specially nucleated holes enable an easy experimental access for temporal and spatial observation.

While fronts retract from the substrate and holes grow, a liquid rim is formed at the three-phase contact line due to conservation of liquid volume. A common phenomenon is the formation of liquid bulges and 'fingers' due to the fact that the liquid rim becomes unstable, similar to the instability of a cylindrical liquid jet that beads up into droplets (e.g. in case of a water tap). This so-called *Rayleigh–Plateau instability* is based on the fact that certain modes of fluctuation become amplified and surface corrugations of a characteristic wavelength become visible. If two holes coalesce, a common ridge builds up, that in the end decays into single droplets due to the same mechanism. The final stage is given by an equilibrium configuration of liquid droplets arranged on the substrate exhibiting a static contact angle. Actually, the final state would be one single droplet, since the Laplace pressure in droplets of different size varies. Yet, a substantial material transport must take place, either through the gas phase or via an equilibrium film between the droplets. This phenomenon is also called *Ostwald ripening*. In polymeric liquids, these transport pathways are usually extremely slow so that a network-like pattern of liquid droplets is already termed 'final stage'. Besides the dynamics and stability of thin liquid films driven by inter-molecular forces, a recent article by Craster and Matar reviews further aspects, such as e.g thermally or surfactant driven flows [11].

In the first part of this topical review, basic concepts from hydrodynamic theories in the bulk situation to corresponding models with regard to confinement are introduced. Polymers are regarded as ideal model liquids due to their low vapor pressure, the available chemical purity and, furthermore, the fact that their viscosity can be controlled in a very reliable manner. By setting the viscosity via temperature,

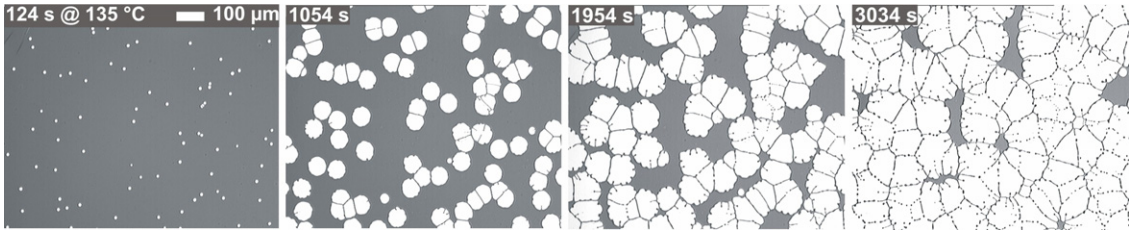

Figure 2. Dewetting of a 80 nm PS(65 kg mol^{-1}) film at $T = 135\,^{\circ}$C from a hydrophobized Si substrate captured by optical microscopy (adapted with permission from [10]. Copyright 2000 by Springer Science + Business Media).

the experimental conditions can be tuned so that dewetting dynamics can be easily captured. Mass conservation can safely be assumed, which consequently simplifies the theoretical description. The dewetting dynamics governed by the driving forces and the mechanisms of energy dissipation will also be discussed with regard to the shape of liquid ridges. The second part summarizes experimental studies concerning the dynamics of two different dewetting geometries: straight front geometry and the growth of holes. The influence of parameters such as dewetting temperature, viscosity and molecular weight of the polymer will be discussed in detail. Moreover, we focus on various scenarios at the solid/liquid interface on the molecular level. Simulations such as, for example, molecular-dynamic (MD) studies help to obtain more information and are supportive to gaining insight into the molecular mechanism of slippage.

2. Basic theoretical concepts

In this section, we aim to describe the main concepts of fluid dynamics, especially in a confined geometry. Depending on the type of liquid, viscous or even viscoelastic effects have to be considered, and deviations from Newtonian behavior might become non-negligible. Since we concentrate in this article on polymer melts, viscosity and viscoelasticity can be varied by chain length and branching of the polymer. An important aspect of a moving liquid is the velocity profile.

2.1. Polymer properties

For a comprehensive understanding of slippage, some important polymer properties such as glass transition temperature, viscosity and viscoelasticity have to be taken into account. Especially in geometries like those in a liquid film, confinement effects are a concern. A detailed description can be found in textbooks [12, 13].

2.1.1. Polymer physics. Polymers are synthesized by polymerization of monomers of molar mass M_{mono}. To characterize the polydispersity of polymer chains in a solution or in a melt, the polydispersity index M_w/M_n is calculated as the ratio of mean values given by the weight M_w and number averaged molecular weight M_n. Polymers are able to change their conformations. The radius of gyration characterizes the spatial dimension of the polymer and is given as the mean square displacement between monomers and the polymer's center of mass. In an isotropic configuration, the shape of the polymer chain can be approximated as a spherical entity. Polystyrene, abbreviated PS, which is commonly used as a melt in dewetting experiments, is a linear homopolymer with $M_{\mathrm{mono}} = 104\ \mathrm{g\,mol^{-1}}$. In addition to other properties concerning the micro-structure of polymer chains such as the tacticity and the architecture (linear, branched, ring-shaped), physical properties are of special interest. If a melt is heated above its glass transition temperature T_{g}, a phase transition from the glassy phase to the liquid phase occurs and the polymer becomes liquid. Randomly structured macromolecules such as atactic polymers avoid the formation of semi-crystalline domains below T_{g} and exhibit a purely amorphous phase. The glass transition of a bulk polymer or of a polymeric thin film can be observed, e.g. via probing its linear expansion coefficient. Although the glass transition is based on a kinematic effect and does not occur due to a rearrangement process of polymer chains. Therefore, the glass transition usually takes place at a specific temperature range and not at an exactly allocable temperature. According to the increased mobility of shorter chains, their glass transition temperature is decreased significantly. For PS with a sufficiently large chain length, $T_{\mathrm{g}} = 100\,^{\circ}$C.

The viscosity η of a polymer melt measures the inner friction of polymer chains and governs the timescale of flow processes. Due to the fact that the mobility of chains increases while the temperature increases, the viscosity decreases. Internal stresses relax and dynamical processes proceed faster. The most common description of the functional dependency of the viscosity η of a polymer on temperature T was developed by Williams, Landel and Ferry:

$$\eta = \eta_{\mathrm{g}} \exp \frac{B(T_{\mathrm{g}} - T)}{f_{\mathrm{g}}(T - T_{\infty})}. \tag{2.1}$$

In this so-called WLF-equation, η_{g} denotes the viscosity at T_{g}, B an empirically obtained constant, T_{∞} the so-called Vogel temperature and f_{g} the free liquid volume fraction.

Besides the above discussed impact of temperature on the viscosity of a polymer melt, the molecular weight M_w also strongly influences η. While M_w increases, the chain mobility decreases and, therefore, the relaxation times and, thus, η increase. For sufficiently small M_w, the Rouse model predicts a linear increase of η for increasing M_w. At this point, another characteristic number of polymer physics has to be introduced: the critical chain length for entanglements M_{c}. Above M_{c}, the polymer chains form chain entanglements exhibiting a specific

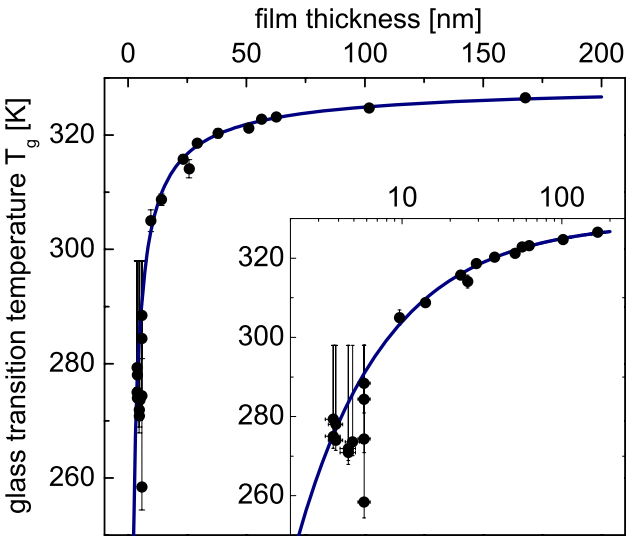

Figure 3. Glass transition temperature T_g of polystyrene films of 2 kg mol^{-1} against film thickness (adapted from [21]).

mean strand length called *entanglement length* M_e. For PS, $M_c = 35$ kg mol^{-1} and $M_e = 17$ kg mol^{-1} is found [12]. According to the reptation model of de Gennes [14], the viscosity increases more strongly in the presence of chain entanglements and an algebraic behavior of $\eta \propto M_w^3$ is expected. Empirically, the linear regime below M_c is well reproduced, above M_c an exponent of 3.4 is experimentally found for different polymers. For a detailed description of chemical and physical properties of polymers, as well as for the Rouse or the reptation theory, we refer to the book *Polymer Physics* by Rubinstein and Colby [12].

2.1.2. Properties in confined geometries. In contrast to the bulk situation, where volume properties of the polymers are measured, liquids in confined geometries, such as a thin film, often show deviations from the behavior in the volume due to additional interface effects. One of these properties is the aforementioned glass transition temperature. It has been shown in numerous studies, that T_g changes with film thickness h. On the one hand, in cases of free-standing or supported films exhibiting no or repulsive interactions with the substrate, $T_g(h)$ decreases with decreasing film thickness [15–18]. On the other hand, Keddie and Jones have shown that an increase in the glass transition temperature with decreasing film thickness is possible for attractive interactions between the substrate and the polymer film [19]. The influence of the interfacial energy on the deviation of T_g from its bulk value has been studied and quantified by Fryer *et al* for different polymers [20]. In the case of PS on a solid support, a significant change of T_g is found for films thinner than 100 nm (see figure 3) [21]. For PS(2k) below 10 nm for instance, the glass transition temperature and the viscosity of the polymer film are affected such that these films are liquid at room temperature and may dewet spinodally.

Several attempts have been made to explain the change of T_g according to the film thickness. Besides interface-related effects such as reorientation of polymer chains or accumulation of chain-ends at the interface, finite-size effects have been proposed to be responsible. Herminghaus *et al* discussed the strain relaxation behavior of thin viscoelastic polymer films with regard to surface melting and the shift of the glass transition temperature [21]. Kawana and Jones studied the thermal expansivity of thin supported polymer films using ellipsometry and attributed their results concerning T_g to a liquid-like surface layer [22], a result that was also found by other authors [23, 24]. Besides confinement effects on T_g, further interface-related phenomena have been studied: Si *et al* have shown that polymers in thin films are less entangled than bulk polymers and that the effective entanglement molecular weight M_e is significantly larger than the bulk value [25].

2.1.3. Viscosity and viscoelasticity. One of the major characteristics of a liquid in general, or a polymer in particular, is its viscosity η. Applying shear stress σ to a liquid usually causes it to react with a strain γ. If stress and strain rate $\dot{\gamma}$ are proportional, the fluid is called *Newtonian*. The constant of proportionality is identified as the viscosity η of the liquid.

$$\sigma = \eta\dot{\gamma}. \tag{2.2}$$

Liquids such as long-chained polymers show a shear-rate-dependent viscosity $\eta(\dot{\gamma})$ due to the fact that the liquid molecules are entangled. If the viscosity increases while shearing the liquid, we call this behavior *shear thickening*, whereas in case of lowered viscosity so-called *shear thinning* is responsible. In contrast to the elastic deformation of a solid, a deformation of a *viscoelastic* liquid might induce an additional flow and can relax on a specific timescale τ. On short timescales ($t < \tau$), the liquid behaves in an elastic, on long timescales ($t > \tau$) in a viscous manner. Strain γ is thereby connected to stress σ via the elastic modulus G of the liquid:

$$\sigma = G\gamma. \tag{2.3}$$

To cover the stress relaxation dynamics of a polymer film, several modeling attempts have been proposed. Mostly, so-called *Maxwell* or *Jeffreys* models are applied. The simplest model is the *Maxwell* model (see figure 4), which assumes a serial connection of a perfectly elastic element (represented by a spring) and a perfectly viscous one (represented by a dashpot). Consequently, the total shear strain γ is given by the sum of the corresponding shear strains γ_e and γ_v of both mechanisms:

$$\gamma = \gamma_e + \gamma_v. \tag{2.4}$$

With (2.3) and (2.2), we get

$$\sigma = G_M\gamma_e = \eta_M\dot{\gamma}_v \tag{2.5}$$

since both react on the same shear stress σ. Therefore, the ratio of viscosity of the viscous element to the elastic modulus of the elastic one can be identified with a specific timescale, the relaxation time τ_M:

$$\tau_M = \frac{\eta_M}{G_M}. \tag{2.6}$$

The relaxation of stress after a step strain γ leads to a time-dependent stress function $\sigma(t)$ for a viscoelastic liquid. Due

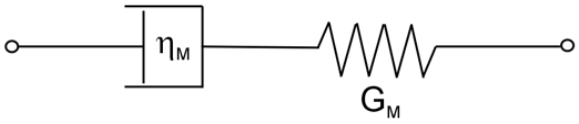

Figure 4. Maxwell model represented by a dashpot and a spring in a serial connection.

to the fact that the total strain γ is constant, a first order differential equation for the time-dependent strain $\gamma_v(t)$ is obtained:

$$\tau_M \dot{\gamma}_v = \gamma - \gamma_v(t). \tag{2.7}$$

Solving this differential equation using the initial condition $\gamma_v(t = 0) = 0$ gives a simple exponential decay of $\sigma(t)$ on the timescale of the stress relaxation time τ_M in the Maxwell model:

$$\begin{aligned} \gamma_e(t) &= \gamma \exp(-t/\tau_M), \\ \sigma(t) &= G_M \gamma_e(t) = G_M \gamma \exp(-t/\tau_M). \end{aligned} \tag{2.8}$$

A situation of special interest is the linear response region: for sufficiently small values of γ, the stress/strain-relation (2.3) is valid and the stress relaxation modulus $G(t)$ is independent of the strain γ. In this regime, a linear superposition of stresses resulting from an infinite number of strain steps can be used to model a steady, simple shear flow of a viscoelastic liquid. For larger applied shear rates, the linear response and the linear superposition fails. The viscosity is still defined as the ratio of stress and strain rate, but it has to be regarded as an apparent viscosity which differs from the above-described 'zero shear rate' viscosity. Polymers with *shear thinning* or *shear thickening* properties can be described by the function

$$\sigma \propto \dot{\gamma}^n, \tag{2.9}$$

where the exponent n can be extracted from experimental data. These type of fluids are also called 'power law fluids'. Moreover, also other non-trivial stress–strain relations can be considered or alternatively non-linear extensions can be applied to the linear *Maxwell* models. In the case of the linear *Jeffreys* model, the stress tensor σ_{ij} relaxes according to the following constitutive relaxation equation:

$$(1 + \lambda_1 \partial_t)\sigma = \eta(1 + \lambda_2 \partial_t)\dot{\gamma}, \tag{2.10}$$

where the strain rate is given by the gradient of the velocity field $\dot{\gamma}_{ij} = \partial_j u_i + \partial_i u_j$. Thus, λ_1 governs the relaxation of stress, whereas λ_2 ($\lambda_2 < \lambda_1$) describes the relaxation of the strain rate, respectively. This model accounts for the viscous and the elastic properties of a fluid and was used by Blossey, Rauscher, Wagner and Münch as a basis for the development of a thin film equation that incorporates viscoelastic effects [26–28]. For a more elaborate description of non-Newtonian flows, we refer e.g. to the corresponding work of Te Nijenhuis *et al* [29].

2.1.4. Reynolds and Weissenberg number. The flow of a liquid can be characterized by specific numbers. One of these numbers is the so-called Reynolds number Re, which describes the ratio of inertia effects to viscous flow contributions. In the case of thin liquid films, Re can be written as

$$Re = \frac{\rho u h}{\eta}, \tag{2.11}$$

where ρ denotes the density of the liquid, u describes the flow velocity and h stands for the film thickness [30]. For thin dewetting polymer films, the Reynolds number is very small, i.e. $Re \ll 1$, and a low-Re lubrication theory can be applied. To quantify and to judge the occurrence of viscoelastic effects versus pure viscous flow, the Weissenberg number Wi has been introduced as

$$Wi = \tau \dot{\gamma}. \tag{2.12}$$

Here, τ denotes the relaxation time and $\dot{\gamma}$ the strain rate as introduced in section 2.1.3. If $Wi \ll 1$, an impact of viscoelasticity on flow dynamics can be neglected and viscous flow dominates.

2.2. Navier–Stokes equations

The Navier–Stokes equations for a Newtonian liquid mark the starting point for the discussion of fluid dynamics in confined geometries. According to conservation of mass, the equation of continuity can be formulated as

$$\partial_t \rho + \nabla \cdot (\rho \mathbf{u}) = 0, \tag{2.13}$$

where $\mathbf{u} = (u_x, u_y, u_z)$ is the velocity field of the fluid. For an incompressible liquid, which implies a temporally and spatially constant liquid density ρ, (2.13) can be simplified to

$$\nabla \mathbf{u} = 0. \tag{2.14}$$

With the conservation of momentum, the Navier–Stokes equations for an incompressible liquid can be written as

$$\rho(\partial_t + \mathbf{u} \cdot \nabla)\mathbf{u} = -\nabla p + \eta \triangle \mathbf{u} + \mathbf{f}, \tag{2.15}$$

with the pressure gradient ∇p and the volume force $\mathbf{f}$ of external fields acting as driving forces for the liquid flow. We already stated that, for small Reynolds numbers, i.e. $Re \ll 1$, the terms on the left-hand side of (2.15) can be neglected as compared to terms describing the pressure gradient, external volume forces and viscous flow. With this, we can simplify (2.15) to the so-called Stokes equation

$$0 = -\nabla p + \eta \triangle \mathbf{u} + \mathbf{f}. \tag{2.16}$$

In section 2.5, we will demonstrate how these basic laws of bulk fluid dynamics can be applied to the flow geometry of a thin film supported by a solid substrate.

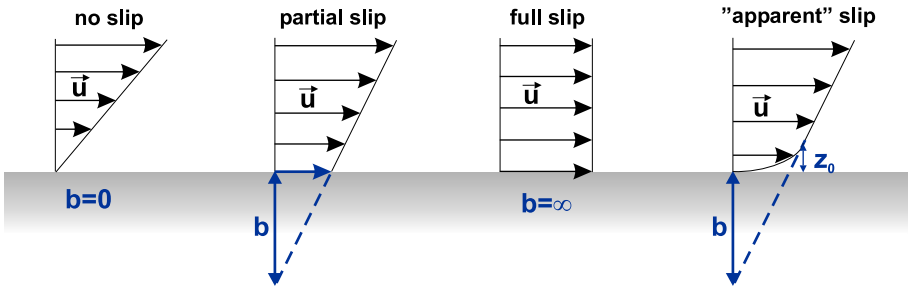

Figure 5. Different velocity profiles in the vicinity of the solid/liquid interface and illustration of the slip (extrapolation) length b. The situation of 'apparent' slip is illustrated on the right: according to a thin liquid layer of thickness z_0 that obtains a significantly reduced viscosity, the slip velocity $u_x|_{z=0}$ is zero, but a substantial slip length is measured.

2.3. Free interface boundary condition

At the free interface of a supported liquid film, i.e. at the liquid/gas or more typically the liquid/air interface, no shear forces can be transferred to the gas phase due to the negligible viscosity of the gas. In general, the stress tensor σ^*_{ij} is given by the stress tension σ_{ij}, see (2.2), and the pressure p:

$$\sigma^*_{ij} = \sigma_{ij} + p\delta_{ij} = \eta(\partial_j u_i + \partial_i u_j) + p\delta_{ij}. \tag{2.17}$$

The tangential $\mathbf{t}$ and normal $\mathbf{n}$ (perpendicular to the interface) components of the stress tensor are:

$$(\sigma^* \cdot \mathbf{n}) \cdot \mathbf{t} = 0 \qquad (\sigma^* \cdot \mathbf{n}) \cdot \mathbf{n} = \gamma_{\mathrm{lv}}\kappa, \tag{2.18}$$

where κ denotes the mean curvature and γ_{lv} the interfacial tension (i.e. the surface tension of the liquid) of the liquid/vapor interface. If the liquid is at rest, i.e. the stationary case $\mathbf{u} = 0$, the latter boundary condition gives the equation for the Laplace pressure p_{L}:

$$p_{\mathrm{L}} = \gamma_{\mathrm{lv}}\kappa = \gamma_{\mathrm{lv}}\left(\frac{1}{R_1} + \frac{1}{R_2}\right). \tag{2.19}$$

R_1 and R_2 are the principal radii of curvature of the free liquid/gas boundary; the appropriate signs of the radii are chosen according to the condition that convex boundaries give positive signs. Such convex liquid/gas boundaries lead to an additional pressure within the liquid due to its surface tension. In the section 2.4, the solid/liquid boundary condition will be discussed, which yields a treatment of slip effects.

2.4. Slip/no-slip boundary condition

2.4.1. Navier slip boundary condition. In contrast to fluid dynamics in a bulk volume, where the assumption that the tangential velocity $\mathbf{u}_\parallel$ at the solid/liquid interface vanishes (*no-slip boundary condition*), confined geometries require a more detailed investigation as slippage becomes important. In 1823, Navier [31] introduced a linear boundary condition: the tangential velocity $\mathbf{u}_\parallel$ is proportional to the normal component of the strain rate tensor; the constant of proportionality is described as the so-called *slip length* b:

$$\mathbf{u}_\parallel = b\mathbf{n} \cdot \dot{\gamma}. \tag{2.20}$$

In the case of simple shear flow in the x-direction, the definition of the slip length can be alternatively written as

$$b = \left.\frac{u_x}{\partial_z u_x}\right|_{z=0} = \frac{u_x \eta}{\sigma} = \frac{\eta}{\xi}, \tag{2.21}$$

where $\xi = \sigma/u_x$ denotes the friction coefficient at the solid/liquid interface. The xy-plane thereby represents the substrate surface. According to these definitions, the slip length can be illustrated as the extrapolation length of the velocity profile 'inside' the substrate, cf figure 5. Moreover, both limiting cases are included within this description: for $b = 0$, we obtain the *no-slip* situation, whereas $b = \infty$ characterizes a *full-slip* situation. The latter case corresponds to 'plug-flow', where the liquid behaves like a solid that slips over the support.

2.4.2. How can one measure the slip length? In recent years, numerous experimental studies have been published using diverse methods to probe the slip length at the boundary of different simple or complex liquids and solid supports. For details concerning these experimental methods, we refer to the review articles by Lauga *et al* [32], Neto *et al* [33] and Bocquet and Barrat [34] (and references therein). To probe the boundary condition, scientists performed either drainage experiments or direct measurements of the local velocity profile using e.g. tracer particles.

In the case of drainage experiments, the liquid is squeezed between two objects, e.g. a flat surface and a colloidal probe at the tip of an AFM cantilever, and the corresponding force for dragging the probe is measured (*colloidal probe AFM*). Alternatively, in a *surface force apparatus (SFA)*, two cylinders arranged perpendicular to each other are brought in closer contact and force/distance measurements are taken to infer the slip length.

The use of tracer particles as a probe of the local flow profile might bring some disadvantages. The chemistry of these particles is usually different from the liquid molecules and their influence on the results might not be negligible. A similar method is called *fluorescence recovery after photobleaching*. In this method, a distinct part of a fluorescent liquid is bleached by a laser pulse and the flow of non-bleached liquid into that part is measured. The disadvantage of this method is that diffusion might be a further parameter that

is difficult to control. Recently, Joly *et al* showed that also thermal motion of confined colloidal tracers in the vicinity of the solid/liquid interface can be used as a probe of slippage without relying on external driving forces [35].

2.4.3. Which parameters influence slippage? Of course, many interesting aspects in the field of micro- and nanofluidics are related to intrinsic parameters that govern slippage of liquid molecules at the solid/liquid interface. For simple liquids on smooth surfaces, the contact angle is one of the main parameters influencing slippage [36–39]. This originates from the effect of molecular interactions between liquid molecules and the solid surface: if the molecular attraction of liquid molecules and surface decreases (and the contact angle thereby increases), slippage is increased. Further studies aim to quantify the impact of roughness [37, 40–42] or topographic structure [43–47] of the surface on slippage. For different roughness length scales, a suppression (see e.g. [37, 40]) or an amplification (see e.g. [43]) of slippage can be observed. Moreover, the shape of molecular liquids itself has been experimentally shown to impact the boundary condition. Schmatko *et al* found significantly larger slip lengths for elongated linear molecules compared to branched molecules [48]. This might be associated with molecular ordering effects [49] and the formation of layers of the fluid in case of the capability of these liquids to align in the vicinity of the interface [50]. Cho *et al* identified the dipole moment of Newtonian liquids at hydrophobic surfaces as a crucial parameter for slip [51]. De Gennes proposed a thin gas layer at the interface of solid surface and liquid as a possible source of large slip lengths [52]. Recently, MD studies for water on hydrophobic surfaces by Huang *et al* revealed a dependence of slippage on the amount of water depletion at the surface and a strong increase of slip with increasing contact angle [53]. Such depletion layers for water in the vicinity of smooth hydrophobic surfaces have also been experimentally observed using scattering techniques [54–57]. Contamination by nanoscale air bubbles (so-called nanobubbles) and its influence on slippage has been controversially discussed in the literature (see e.g. [58–61]). In the case of more complex liquids, such as polymer melts, further concepts come into play. They will be illustrated in section 3.4.

2.5. Thin film equation for Newtonian liquids

2.5.1. Derivation. Confining the flow of a liquid to the geometry of a thin film, we can assume that the velocity contribution perpendicular to the substrate is much smaller than the parallel one. Furthermore, the lateral length scale of film thickness variations is much smaller than the film thickness itself. On the basis of these assumptions, Oron *et al* [62] developed a thin film equation from the rather complex equations of motion, (2.13) and (2.15). In cases of film thicknesses smaller than the capillary length $l_c = \sqrt{\gamma_{lv}/\rho g}$, (which is typically on the order of magnitude of 1 mm) (2.16) can be written as

$$0 = -\nabla(p + \phi'(h)) + \eta \triangle \mathbf{u}. \tag{2.22}$$

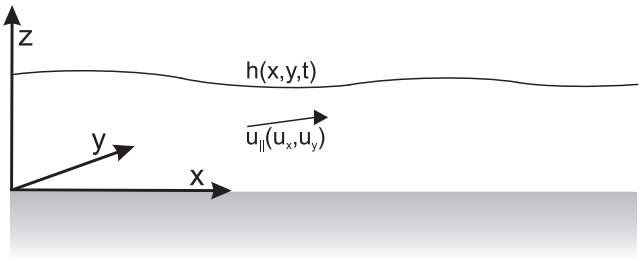

Figure 6. Illustration of the nomenclature of the thin film length scales (x and y are parallel to the substrate) and the velocity contribution $\mathbf{u}_\parallel = (u_x, u_y)$.

Additional external fields such as gravitation can be neglected, but a secondary contribution $\phi'(h)$, the *disjoining pressure*, has been added to the capillary pressure p. The disjoining pressure originates from molecular interactions of the fluid molecules with the substrate. The effective interface potential $\phi(h)$ summarizes the inter-molecular interactions and describes the energy that is required to bring two interfaces from infinity to the finite distance h. As already discussed in section 1, the stability of a thin liquid film is also governed by $\phi(h)$. For a further description of thin film stability, we refer to [8] and the references therein.

The derivation of a thin film equation for Newtonian liquids starts with the kinematic condition

$$\partial_t h = -\nabla_\parallel \int_0^h \mathbf{u}_\parallel \, \mathrm{d}z, \tag{2.23}$$

i.e. the coupling of the time derivative of $h(x, y, t)$ to the flow field, where the index $\parallel$ in general denotes the components parallel to the substrate ($\nabla_\parallel = (\partial_x, \partial_y)$ and $\mathbf{u}_\parallel = (u_x, u_y)$), as illustrated in figure 6.

For thin liquid films, film thickness variations on the lateral scale $\mathbb{L}$ are much larger than the length scale of the film thickness $\mathbb{H}$. Introducing the parameter $\epsilon = \mathbb{H}/\mathbb{L} \ll 1$ yields the *lubrication approximation* and is used in the following to re-scale the variables to dimensionless values. In a first approximation, linearized equations are obtained while neglecting all terms of the order $\mathrm{O}(\epsilon^2)$. For reasons of simplicity and due to translational invariance in the surface plane, a one-dimensional geometry is used:

$$\begin{gathered} \partial_x(p + \phi') = \partial_z^2 u_x, \qquad \partial_z(p + \phi') = 0, \\ \partial_x u_x + \partial_z u_z = 0. \end{gathered} \tag{2.24}$$

While the substrate is supposed to be impenetrable for the liquid, i.e. $u_z = 0$ for $z = 0$, friction at the interface implies a velocity gradient $\partial_z u_x = u_x/b$ for $z = 0$. Moreover, the tangential and normal boundary condition at the free interface, i.e. $z = h(x)$, can be simplified in the following manner:

$$\partial_z u_x = 0, \qquad p + \partial_x^2 h = 0. \tag{2.25}$$

From (2.24) and the boundary conditions, the velocity profile $u_x(z)$ can be obtained. Using the kinematic

Table 1. Summary of lubrication models for Newtonian flow and different slip situations.

Model	Validity	Equation	Limiting cases	Reference
Weak-slip	$b \ll h$	(2.26), (2.27)	$b \to 0$ (no-slip) $b \to \infty$ (intermediate-slip)	[62]
Strong-slip	$b \gg h$	(2.28)	$\beta \to 0$ (intermediate-slip) $\beta \to \infty$ ('free'-slip)	[63, 30]

condition (2.23), the equation of motion for thin films in three dimensions is derived:

$$\partial_t h = -\nabla[m(h)\nabla(\gamma_{\mathrm{lv}}\triangle h - \phi'(h))], \tag{2.26}$$

where $m(h)$ denotes the mobility given by

$$m(h) = \frac{1}{3\eta}(h^3 + 3bh^2). \tag{2.27}$$

2.5.2. Lubrication models including slippage. As discussed in section 2.5.1, the derivation of the thin film equation is based on the lubrication approximation and the re-scaling of relevant values in ϵ. As a consequence, the slip length b is supposed to obtain values smaller than the film thickness h, i.e. $b \ll h$. To extend this so-called *weak-slip* situation with regard to larger slip $b \gg h$, Münch *et al* [30] and Kargupta *et al* [63] independently developed *strong-slip* models. Therefore, the slip length is defined as $b = \beta/\epsilon^2$. The corresponding equation of motion together with the kinematic condition in one dimension for a Newtonian thin liquid film read as

$$\begin{gathered} u = \frac{2b}{\eta}\partial_x(2\eta h\partial_x u) + \frac{bh}{\eta}\partial_x(\gamma_{\mathrm{lv}}\partial_x^2 h - \phi'(h)) \\ \partial_t h = -\partial_x(hu). \end{gathered} \tag{2.28}$$

In fact, a family of lubrication models, cf table 1, accounting for different slip situations have been derived. In the limit $b \to 0$, i.e. the *no-slip* situation, the mobility is given by $m(h) = h^3/3\eta$. If the slip length is in the range of the film thickness $b \sim h$, the mobility in the corresponding *intermediate-slip* model is $m(h) = bh^2/\eta$. Recently, Fetzer *et al* [64] derived a more generalized model based on the full Stokes equations, developed up to third order of a Taylor expansion. The authors were able to show that this model is in accordance with numerical simulations of the full hydrodynamic equations and is not restricted to a certain slip regime, like the aforementioned lubrication models.

2.5.3. Lubrication models including viscoelasticity. In the meantime, the derivation of a thin film equation for the weak-slip case including linear viscoelastic effects of Jeffreys type (such as described by equation (2.10) in section 2.1.3) has been achieved (see [26]). To cover relaxation dynamics of the stress tensor σ, an additional term $\nabla \cdot \sigma$ on the right-hand side of (2.22) has to be included to the aforementioned model for Newtonian liquids. Furthermore, the treatment of linear viscoelastic effects was also achieved for the strong-slip situation by Blossey *et al* [27]. To summarize these extensions, the essential result is the fact that linear viscoelastic effects are absent in the weak-slip case and the Newtonian thin film model is still valid. The strong-slip situation, however, is more complicated. Slippage and viscoelasticity are combined and strongly affect the corresponding equations. In the meantime, the authors were able to fully incorporate the non-linearities of the co-rotational Jeffreys model for viscoelastic relaxation into their thin film model [28].

The extensions of the aforementioned thin film models for different slip conditions, with or without the presence of viscoelastic relaxation (Newtonian and non-Newtonian models), affect, on the one hand, the rupture conditions, but also on the other hand, the shape of a liquid ridge. These two phenomena will be discussed in the next two subsections. An elaborate description of these theoretical aspects can be found in a recent review article by Blossey [65].

2.5.4. Application I—spinodal dewetting. One of the main applications of the theoretical thin film models is the dewetting of thin polymer films. As introduced in section 1, and illustrated by figure 1, the stability of a thin liquid film is governed by the effective interface potential. Basically, long-range attractive van der Waals forces add to short-range repulsive forces. Due to the planar geometry of two interfaces of distance d, the van der Waals contribution to the potential is $\phi(d)_{\mathrm{vdW}} \propto -A/d^2$, where A is the Hamaker constant. For the description of the explicit calculation of Hamaker constants from the dielectric functions of the involved materials, we refer to [8] and to the book by Israelachvili [66]. Experimental systems often exhibit multi-layer situations, cf figure 7. A hydrophobic film and/or an oxide layer of distinct thicknesses d_i exhibiting Hamaker constants A_i require a superposition of contributions to the potential:

$$\phi(d)_{\mathrm{vdw}} = -\frac{A_1}{12\pi d^2} - \frac{A_2 - A_1}{12\pi(d + d_1)^2} - \frac{A_3 - A_2}{12\pi(d + d_1 + d_2)^2}. \tag{2.29}$$

Consequently, the shape of the effective interface potential (and thereby also the thin film stability) is governed by the set of Hamaker constants A_i and film thicknesses d_i. E.g. for a thin PS film of thickness h on a Si substrate with a native oxide layer of 2.4 nm, $\phi(h)$ shows a global minimum at an equilibrium film thickness h_{eq} (cf figure 8). Moreover, a local maximum at $h > h_{\mathrm{eq}}$ is found.

If the PS film is sufficiently thin ($\phi''(h) < 0$), it may become unstable due to the amplification of thermally induced capillary waves. To track the evolution of small fluctuations of the film thickness h, i.e. $f(\mathbf{x}, t) = h(\mathbf{x}, t) - h$ with $f(\mathbf{x}, t) \ll h$, a Fourier transform of the linearized thin film equation (2.26) has to be performed. The amplitudes of the capillary waves grow exponentially in time. Their growth rate α can be calculated as a function of the wavenumber q and depends on the sign of the local curvature of the interface potential. If the second derivative of the effective interface potential ϕ'' at the film thickness h is positive, α is negative

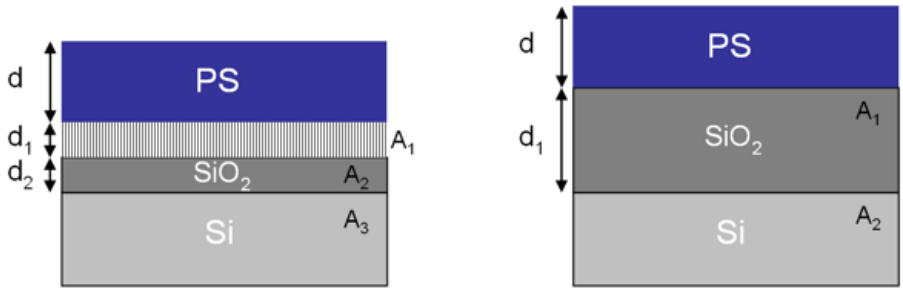

Figure 7. Two examples of polystyrene films prepared on multi-layer substrates. Left: silicon wafer with a native oxide layer covered with a hydrophobic layer (e.g. a self-assembled monolayer (SAM)). Right: silicon wafer with an increased (compared to a native silicon oxide) oxide layer thickness. A_1 denotes the Hamaker constant for the respective layer.

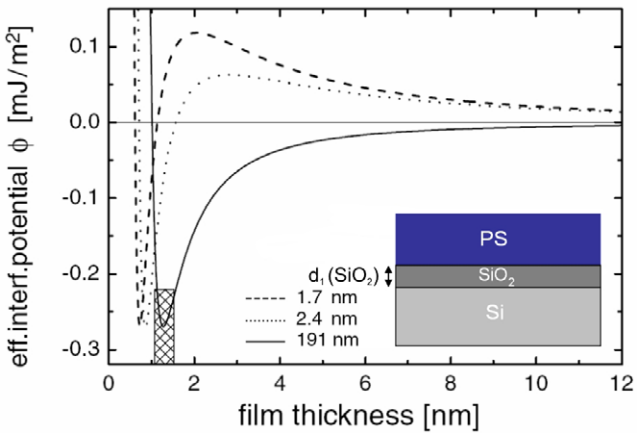

Figure 8. Effective interface potential $\phi(h)$, obtained from experimental data, plotted against the thickness h of a thin PS film prepared on silicon wafers with different oxide layer thicknesses d_1 (adapted from [7]). The cross-hatched rectangle marks the error for h_{eq} and the depth of the global minimum.

for all q and the amplitudes of the capillary waves are damped. If $\phi'' < 0$, the growth rate α is positive for a certain range of wavenumbers up to a critical wavenumber q_c and capillary waves are amplified. The wavenumber that corresponds to the maximum value of α, and therefore exhibits the fastest amplification, is called the preferred wavenumber q_0 and is connected to the preferred wavelength $\lambda_0 = 2\pi/q_0$. The latter is also called the spinodal wavelength and can be written as

$$\lambda_0 = \sqrt{\frac{8\pi^2\gamma_{lv}}{-\phi''(h)}}. \tag{2.30}$$

The spinodal dewetting process can be monitored, e.g. by atomic force microscopy (AFM), as shown in figure 9. By measuring λ_0 as a function of film thickness, $\phi''(h)$ can be inferred and conclusions can be drawn with regard to the effective interface potential $\phi(h)$ [7]. For further details concerning stability of thin films, we refer to [8] and references therein.

Using the strong-slip model while taking slip into account (2.28), Rauscher *et al* could theoretically show that slippage is supposed to influence the capillary wave spectrum due to a different mobility at the solid/liquid interface [68]. The position of the maximum q_0 shifts to smaller wavenumbers and larger wavelengths for increasing slip length. As for today, to the best of our knowledge, experimental studies concerning the impact of slippage on the spinodal wavelength are not available.

The description of the influence of thermal noise on the temporal and spatial dynamics of spinodally dewetting thin polymer films has been recently achieved by Fetzer *et al* [69]. A stochastic Navier–Stokes equation, with an additional random stress fluctuation tensor that accounts for thermal molecular motion, is utilized to model the flow while assuming a no-slip boundary condition at the solid/liquid interface. The stochastic model matches the experimentally observed spectrum of capillary waves and thermal fluctuations cause the coarsening of typical length scales.

2.5.5. Application II—shape of a dewetting rim. Aside from the implications on spinodal dewetting, the one-dimensional thin film model has been successfully applied to the shape of the rim along the perimeter of e.g. nucleated holes. Experimentally, researchers have studied and observed different types of rim profiles [70–72]. As shown in figure 10, profiles either decay monotonically into the undisturbed film or they show a more symmetrical profile exhibiting a trough (termed 'oscillatory shape'). If the depth of this trough is in the range of the film thickness, a ring of *satellite holes* can be generated [73, 74].

The shape of a dewetting rim can be understood by the aforementioned thin film theory for Newtonian liquids: introducing a small perturbation $\delta h(x,t) \ll h$ of the film thickness $h(x,t)$ and small velocities $u(x,t)$ leads to linearized thin film equations that describe the temporal and spatial evolution of δh. Therefore, the disjoining pressure $\phi'(h)$ can be neglected due to the fact that films thicker than 10 nm are considered. To obtain stationary solutions of the linearized equations, a frame that is co-moving with the rim $\zeta(x,t) = x - s(t)$ is introduced. Thus, $s(t)$ denotes the position of the three-phase contact line; $\dot{s}$ stands for the dewetting velocity V as described in the next sections. Fetzer *et al* used a normal modes ansatz $\delta h(\zeta) = \delta h_0 \exp k\zeta$ and $u(\zeta) = u_0 \exp k\zeta$ in the linear stability analysis, which leads to a characteristic polynomial of third order. Depending on

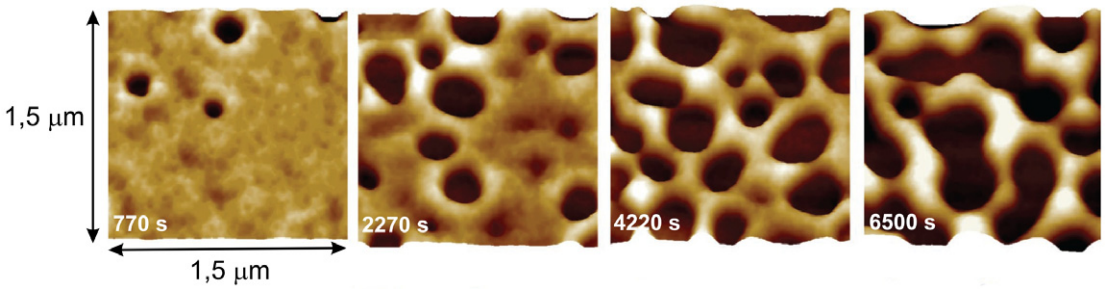

Figure 9. *In situ* atomic force microscopy (AFM) images of a spinodally dewetting 3.9(2) nm PS(2 kg mol^{-1}) film at elevated temperature of $T = 53\,^{\circ}$C (corresponding annealing times are given in the pictures) on a Si wafer with a thick (191 nm) oxide layer (adapted from [67]).

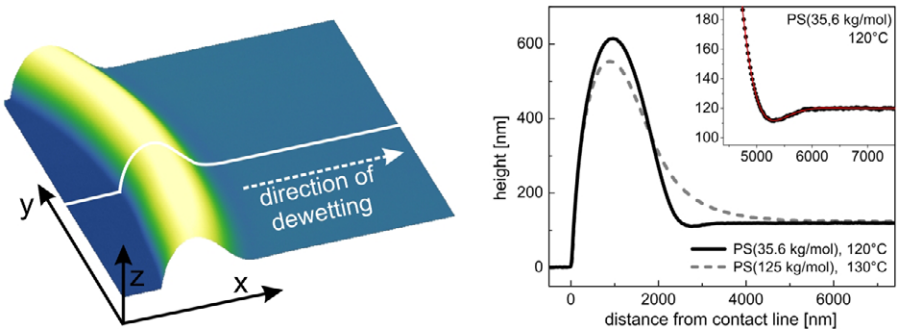

Figure 10. Left: 10 μm $\times$ 10 μm AFM image of a liquid rim formed during hole growth in a PS film dewetting from a hydrophobic substrate, a Si wafer covered with a 21 nm hydrophobic Teflon coating (AF 1600). The solid white line exemplarily marks one AFM scan line. Right: AFM cross-sections of rims in PS films of different molecular weight on AF 1600: for PS(35.6 kg mol^{-1}) at 120 °C, a trough is observed (as can be clearly seen in the inset) and for PS(125 kg mol^{-1}) at 130 °C, a monotonically decying rim is found.

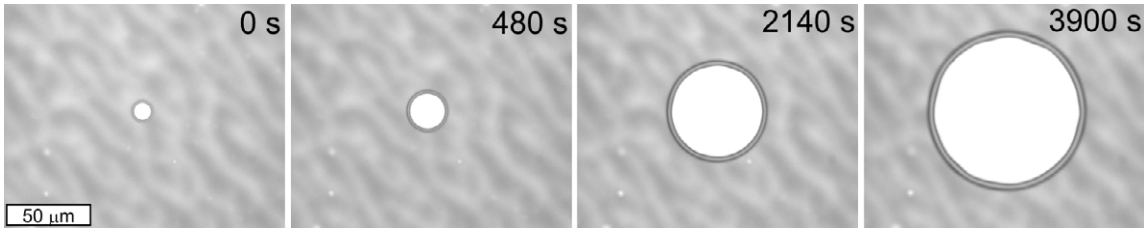

Figure 11. Temporal series of optical micrographs showing the growth of a hole in a 120 nm PS(13.7 kg mol^{-1}) film at $T = 120\,^{\circ}$C prepared on a Si wafer covered with a 21 nm hydrophobic Teflon® coating (AF1600). Note that the AF 1600 coating shows small thickness variations that have proved not to influence dewetting i.e. the curvature of the holes and the shape of straight fronts are not affected. In the last stage of hole growth (right image) perturbations of the three-phase contact line (according to the liquid rim instability) become visible.

the ratio of slip length to film thickness b/h and on the capillary number $Ca = \eta\dot{s}/\gamma_{lv}$, the parameter k obtains complex or real solutions. Fetzer and co-workers successfully identified the morphological transition from oscillatory to monotonically decaying rims and were able to extract slip lengths and capillary numbers from diverse experiments on dewetting surfaces [75, 76, 64, 77].

3. Flow dynamics of thin polymer films—experimental studies and theoretical models

One of the main aspects of experimental studies concerning the flow dynamics of thin polymer films is to obtain a comprehensive view on the molecular mechanisms of slippage and on the responsible parameters. Although these insights are rather indirect, several models have been proposed to explain diverse experimental results. In this section, we will focus on these studies, with special regard to the proposed mechanisms of slippage at the solid/polymer interface. In general, we have to distinguish two different dewetting geometries: growth of holes (cf figure 11) and receding straight fronts. In addition to driving forces, dissipation mechanisms have to be considered.

3.1. Dewetting dynamics—driving forces

According to the description of the effective interface potential in section 2.5.4, a global minimum of $\phi(h)$ occurs at h_{eq} in case of unstable or metastable films. This means that the film will thin out until a thickness of h_{eq} is reached. In other words, a thin wetting layer remains on top of the substrate, if $h_{eq} > 0$

and if h_{eq} has a size that is not below the size of the molecules[1]. After dewetting has taken place (the dynamics of which are not covered by $\phi(h)$ but depend on viscosity, viscoelasticity, contact angle and the solid/liquid boundary condition), single droplets remain on top of the wetting layer. The droplets—in equilibrium—exhibit Young's contact angle θ_Y. Parallel to Young's equation that characterizes the contact angle via the involved surface tensions, another characteristic parameter can be defined to specify the wettability of a surface by a liquid. This is the so-called *spreading parameter* S given by

$$S = \gamma_{sv} - (\gamma_{sl} + \gamma_{lv} + \phi(h_{eq})), \tag{3.1}$$

where γ_{ij} denotes the interface tension of the solid (s), liquid (l) and the vapor (v) phase. S describes the energetic difference per unit area between a dry surface and a surface that is covered by a liquid layer. Consequently, if $S < 0$ the system can gain energy by reducing the contact area with the substrate. Hence, the liquid forms a dynamic contact angle $\theta_d = \theta_Y/\sqrt{2}$ at the three-phase contact line [81].

The link between the contact angle in equilibrium and the depth of the minimum of the effective interface potential becomes obvious, if the equation for Young's contact angle is inserted into (3.1):

$$\phi(h_{eq}) = \gamma_{lv}(\cos\theta_Y - 1) = S. \tag{3.2}$$

Driving forces for wetting and dewetting are capillary forces (see [78]). The capillary force per unit length of the contact line is in general given by

$$\frac{F_c}{l} = \gamma_{lv}(\cos\theta_Y - \cos\theta_d). \tag{3.3}$$

As long as $\theta_d < \theta_Y$ remains valid, the capillary force is negative and the three-phase contact line recedes; the liquid film dewets. Dewetting ends as soon as droplets exhibit their Young's contact angle θ_Y on the surface. During dewetting, a rim is formed from accumulated material and retracts from the substrate while growing further. De Gennes developed a theoretical description of the resulting driving force for dewetting [78].

On the 'dry' side of the rim, which denotes the side where the three-phase contact line is located, a negative capillary force pulls at the contact line:

$$\frac{F_c}{l} = S + \gamma_{lv}(1 - \cos\theta_d). \tag{3.4}$$

On the other side, where the rim decays into the liquid film (the 'wet' side of the rim), a positive capillary force occurs:

$$\frac{F_c}{l} = \gamma_{lv}(1 - \cos\theta_d). \tag{3.5}$$

We have to remark that in experimental systems, the Laplace pressure of course avoids edges and, therefore, forces the dry side of the rim to decay smoothly into the film. Summing up both forces per unit length gives the effective driving force for retracting contact lines in dewetting systems:

$$\frac{F_c}{l} = |S| = \gamma_{lv}(1 - \cos\theta_Y) \simeq \frac{1}{2}\gamma_{lv}\theta_Y. \tag{3.6}$$

Therefore, it is assumed that the system is in a quasi-stationary state, which means that changes in the shape of the rim occur much more slowly than the dewetting velocity. All in all, this result implies that the driving force for dewetting is given by the absolute value of the spreading parameter, which solely depends on the surface tension γ_{lv} of the liquid (a property which is purely inherent to the liquid) and Young's contact angle of the liquid on the surface. The same conclusion is drawn if considering energies instead of driving forces. The depth of the minimum of the effective interface potential $\phi(h)$ is equal to S and gives the energy per unit area that is set free during dewetting [79]. Consequently, S also stands for the force per unit length of the contact line (see (3.6)).

3.2. Dewetting dynamics—dissipation mechanisms

In section 3.1, we focused on the driving forces for dewetting. The experimentally observed dynamics represents a force balance of driving forces and friction forces. The resulting dewetting velocity V is connected to the spreading parameter S and the occurring energy dissipation mechanisms (F_i gives the friction force per unit length of the contact line) and their corresponding velocity contributions v_i via the power balance

$$|S|V = \sum_i F_i v_i. \tag{3.7}$$

In the case of dissipation due to viscous friction within the liquid (F_v) and dissipation due to friction of liquid molecules at the solid/liquid interface (F_s), i.e. slippage with a finite velocity $v_s = u|_{z=0}$, we end up with the following balance (the index v stands for 'viscous', s denotes 'slip'):

$$|S|V = F_v v_v + F_s v_s. \tag{3.8}$$

3.2.1. Viscous friction. According to the work of Brochard-Wyart *et al* [80], the no-slip boundary condition for fluid flow implies a friction force that is proportional to the liquid viscosity and the dewetting velocity v, and means that the dissipation is solely due to viscous friction within the liquid. The largest strain rates occur in the direct vicinity of the three-phase contact line. The dissipation is therefore mainly independent from the size of the dewetting rim. However, the flow geometry (given by the dynamic contact angle θ_d) at the contact line influences viscous dissipation. In the case of pure viscous flow $V = v_v$, the following expression for the velocity contribution is obtained for viscous flow [80]:

$$v_v = C_v(\theta_d)\frac{|S|}{\eta}. \tag{3.9}$$

$C_v(\theta_d)$ denotes the constant of proportionality and displays a measurement for the flow field in the vicinity of the contact line. According to the description of Redon *et al* [81], the

[1] Note that the concept of the effective interface potential is a continuum approach. It may fail if molecular sized phenomena are to be captured, such as extremely thin films close to the size of the molecules.

velocity in case of viscous dissipation strongly depends on θ_Y and can also be written as

$$v_v \propto \frac{\gamma_{lv}}{\eta}\theta_Y^3, \tag{3.10}$$

where the constant of proportionality accounts for the flow singularity near the contact line. In detail, this constant represents a logarithmic factor that includes i.e. a short-distance cutoff and accounts for the fact that viscous dissipation diverges near the contact line. Moreover, a small impact of the slip length b on this logarithmic factor has been experimentally found [81] by variation of molecular weight M_w (cf (3.12)) by Redon [82]. Consequently, solely in the case of a no-slip boundary condition, the constant of proportionality in (3.10) and also $C_v(\theta_d)$ in (3.9) is purely independent of slip.

For growing holes of radius R and dewetting velocity $V = dR/dt$, integration of (3.9) gives a linear proportionality of the radius versus dewetting time t:

$$R \propto t. \tag{3.11}$$

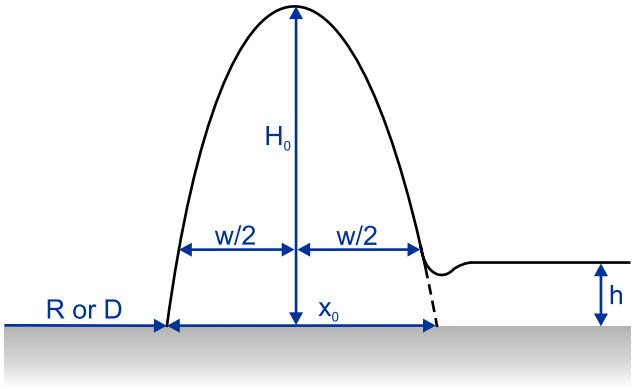

Figure 12. Schematic representation of a rim cross-section illustrating the rim width w (usually obtained as the distance between the three-phase contact line and the position where the rim height is dropped to $1.1h$), the distance x_0 for a given film thickness h and hole radius R (or dewetted distance D of a straight front). (The height scale in the sketch is exaggerated as compared to the lateral length scale.)

3.2.2. Slippage—friction at the solid/liquid interface. Apart from viscous dissipation within the rim, de Gennes expected a long-chained polymer film to exhibit an exceptional amount of slippage. For entangled polymer melts on a non-adsorbing surface, de Gennes stated that the slip length should strongly increase with the chain length of the polymer [83]:

$$b = a\frac{N^3}{N_e^2}, \tag{3.12}$$

where a is the size of the monomer, N the polymerization index and N_e the entanglement length. In cases of dominating slippage, a minor contribution of viscous dissipation is expected due to very small stresses within the rim. The corresponding analytical model (see [80, 82]) is based on the linear friction force per unit length of the contact line given by $F_s \propto \xi v_s$. Dissipation occurs along the distance of the solid/liquid interface, where liquid molecules are moved over the substrate. In general, this distance is identified as the width w of the rim (cf figure 12).

Consequently, $F_s \propto w$ can be assumed. If the slip length is introduced according to Navier's model by $b = \eta/\xi$ (see (2.21) in section 2.4), the slip velocity contribution v_s is given by

$$v_s = \frac{1}{3}\frac{|S|}{\eta}\frac{b}{w}. \tag{3.13}$$

Let us consider the conservation of mass for a growing hole of radius R,

$$\pi(R + x_0)^2 h = 2\pi Q(R + w/2), \tag{3.14}$$

and for a straight dewetting front of dewetted distance D,

$$(D + x_0)lh = Ql, \tag{3.15}$$

where x_0 stands for the distance as depicted in figure 12, Q denotes the cross sectional area of a rim (approximated as a half-circle[2], i.e. $Q = \pi(x_0/2)^2 \approx \pi(w/2)^2$), and l is the length of a straight front, which cancels out. Based on the assumption of self-similar growing rims and the fact that $x_0/R \ll 1$ and $x_0/D \ll 1$, the width of the rim $w \propto \sqrt{h}\sqrt{R}$ for both geometries. The constant of proportionality, however, which we name C_s in the following, depends on the shape of the rim and, furthermore, on the dewetting geometry itself:

$$w = C_s\sqrt{h}\sqrt{R}. \tag{3.16}$$

Values for C_s can be obtained collecting a temporal series of AFM snapshots of rim profiles and fitting (3.16) to the measured rim width w plotted versus the hole radius R. The initial film thickness h can also be measured by AFM. Of course, the validity of this simplified model, and especially the approximation $w \approx x_0$, becomes questionable for asymmetric rims and should lead to systematic differences in C_s. We point out that, as described in section 2.5.5, the degree of asymmetry of the cross-section of the rim is strongly correlated to the capillary number and the ratio of slip length to film thickness. Replacing the above-derived relation of rim width w and hole radius R in (3.13) gives the slip velocity contribution in terms of the hole radius R for purely slipping liquids:

$$v_s = \frac{1}{3}\frac{|S|}{\eta}\frac{b}{C_s\sqrt{h}}\frac{1}{\sqrt{R}}. \tag{3.17}$$

Via integration, a characteristic growth law for the radius R of a dewetting hole with time t is found (separation of variables),

$$R \propto t^{2/3}. \tag{3.18}$$

Using the lubrication models described in section 2.5, Münch compared numerical simulations of polymer melts

[2] Note that usually a dynamic contact angle $\theta_d < 90°$ at the three-phase contact line is obtained in experiments. The difference between a segment of a circle and the half-circle approximation is marginal and contributes to the constant of proportionality C_s.

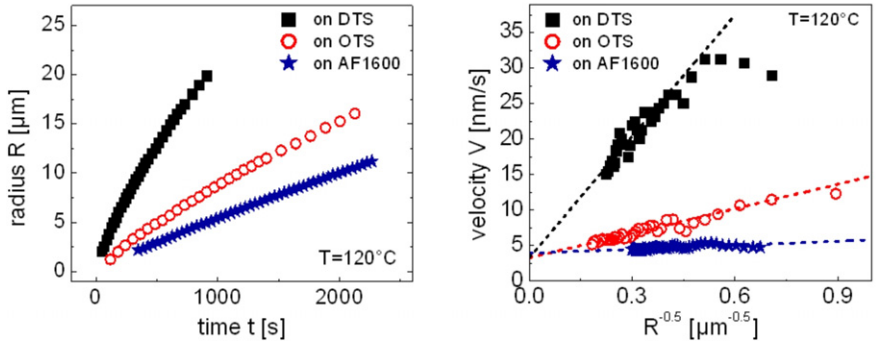

Figure 13. Left: optical measurement of the hole radius versus time in 130 nm PS (13.7 kg mol^{-1}) films on different substrates. Right: plot of the dewetting velocity V versus $1/\sqrt{R}$. Within the error bar, the y-axis intercept of the extrapolated experimental data points is identical for all substrates. The difference in the slope K indicates substantial differences in slip for dewetting PS (adapted from [86] and [87]).

dewetting from hydrophobized substrates to the above-described dewetting dynamics obtained from scaling arguments (based on energy balances) [84]: in the no-slip situation (mobility $m(h) \propto h^3$), an exponent $\alpha = 0.913$ is reported instead of one. The deviation is traced back to the fact that the logarithmic factor in the constant of proportionality of equation (3.10) also depends on the width of the rim (which evolves with time t). Numerical simulations of the slip-dominated case ($m(h) \propto h^2$) give $\alpha = 0.661$, which captures $\alpha = 2/3$ very well.

3.2.3. Models based on the superposition of dissipation mechanisms. Considering the models derived before for pure viscous flow and for pure slippage, a combination of these models seems to be reasonable for situations where viscous dissipation and dissipation at the solid/liquid interface act together. Jacobs *et al* proposed an additive superposition of the corresponding velocity contributions, i.e. $V = v_s + v_v$ [85], according to the fact that both mechanisms counteract the same driving force $|S|$. Separation of variables leads to the implicit function:

$$t - t_0 = \frac{K_v}{|S|}\left(R - 2\frac{K_v}{K_s}\sqrt{R} + 2\left(\frac{K_v}{K_s}\right)^2 \ln\left(1 + \frac{K_s\sqrt{R}}{K_v}\right)\right) \tag{3.19}$$

with

$$K_v = \frac{\eta}{C_v(\theta_d)}, \qquad K_s = \frac{3\eta}{b}\frac{w}{\sqrt{R}}, \qquad \frac{K_v}{K_s} \propto b\sqrt{R}. \tag{3.20}$$

In that notation, the velocity contributions are given by $v_v = |S|/K_v$ and $v_s = |S|/(\sqrt{R}K_v)$. One of the preconditions of this superposition was the successful inclusion of both border cases: for $b \to 0$, $R \propto t$ is obtained, whereas for $b \to \infty$, $R \propto t^{2/3}$ follows.

As a more practicable alternative for fitting this relation between radius R and time t to experimental data (typical data is shown in figure 13), Fetzer and Jacobs recently proposed a simpler way of visualizing slip effects [86]: according to the additive superposition, the dewetting velocity can be written in terms of

$$V = v_v + \frac{K}{\sqrt{R}}, \qquad K = \frac{1}{3}\frac{|S|}{\eta}\frac{b}{C_s\sqrt{h}} \tag{3.21}$$

which leads to a linear relationship when plotting the dewetting velocity v versus $1/\sqrt{R}$ (cf figure 13). Then, the y-axis intercept of the straight line can be identified as the viscous velocity contribution v_v, whereas the slope K is connected to the slip length, as illustrated in (3.21). The validity of this model, which assumes the linear superposition of velocity contributions, was checked by plotting the viscous velocity contribution v_v versus the reciprocal viscosity η. An excellent correlation has been demonstrated in view of melt viscosity data obtained from independent measurements. Moreover, the slope has been used to calculate the slip length b. In the experiments, substantial differences in slip lengths for different substrates (cf figure 13) at identical liquid properties were able to be detected [86].

3.2.4. Molecular-kinetic theory and further approaches. Besides theoretical models based on continuum hydrodynamics (see (3.2.1)), contact line dynamics, such as the spreading of a liquid droplet on a planar surface, has been analyzed according to the *molecular-kinetic theory* (MKT) [88–90]. The movement of a contact line is described as an activated rate process where the liquid molecules close to the substrate jump from one potential well to another. The resulting contact line friction coefficient is proportional i.a. to the viscosity η of the liquid and to the exponential of the reversible work of adhesion $\gamma_{lv}(1 + \cos\theta_Y)/k_BT$. As a consequence, increasing the temperature reduces the friction coefficient and increases the velocity. In the case of a squalane droplet spreading on gold surfaces covered with different self-assembled monolayers (SAM) of thiols, the corresponding contact line friction coefficient proves to increase linearly with the chain length of the SAM [91]. SAM surfaces have also been the subject of friction experiments using AFM tips. Barrena *et al* explained discrete changes in the frictional behavior with discrete molecular tilts of the chains of the SAM [92]. Viscoelastic deformation of the substrate at the contact line due to the normal component of the liquid surface tension has also attracted attention with

regard to fluid dynamics on the nanoscale and energy dissipation. The phenomenon of a reduced velocity of contact line displacements compared to a corresponding non-deformable substrate (termed 'viscoelastic braking') was extensively studied and described by Shanahan and Carré [93–97]. In this context, Long *et al* theoretically examined the static and dynamic wetting properties of liquids on thin rubber films [98] and grafted polymer layers [99]. To the best of our knowledge, there is, to date, no experimental evidence of deformations and tilting on the molecular scale in the case of SAM surfaces due to retracting contact lines of a dewetting polymer film. However, dewetting on soft deformable rubber surfaces has recently been shown to be influenced by viscoelastic deformations of the substrate [100]. In the case of non-volatile liquids such as polymers, evaporation into, and condensation from, the vapor phase can be excluded as the relevant mechanism of energy dissipation.

3.3. Dynamics of growing holes

Besides very early theoretical and experimental studies of thin film rupture [5, 101–106], one of the first studies concerning dewetting experiments had been published by Redon *et al* [81]. Films of alkanes and polydimethylsiloxane (PDMS) have been prepared on different hydrophobized silicon wafers. The authors observed a constant dewetting velocity, which was inversely proportional to the viscosity and very sensitive to the equilibrium contact angle of the liquid on a corresponding surface. In 1994, Redon *et al* investigated the dewetting of PDMS films of different thicknesses on silanized hydrophobic surfaces [82]. They found that, for films larger than 10 μm, a constant dewetting velocity is found, whereas $R(t) \propto t^{2/3}$ in films thinner than 1 μm is observed. These results corroborate the models represented by (3.11) and (3.18) and indicate that for sufficiently thick films ($h \gg b$) viscous dissipation dominates, whereas slippage becomes relevant in the case of thin films ($h < b$) [82].

3.3.1. Stages of dewetting. While studying the growth of holes, Brochard-Wyart *et al* proposed a set of subsequent stages that can be attributed to distinct growth laws [107]: starting with the birth of the hole, the radius of the hole is supposed to grow exponentially with time, i.e. $R(t) \propto \exp(t/\tau)$, as long as the radius R is smaller than $R_c \approx \sqrt{bh}$. Experimentally, Masson *et al* [108] found relaxation times orders of magnitude larger than the largest translational reptation times expected. For $R_c < R < R_c' \approx b$, the rim is formed and viscous dissipation dominates the hole growth dynamics, i.e. $R \propto t$. The special case of $R \gg R_c = \sqrt{bh}$ moreover gives an analytic expression for the hole growth:

$$R(t) \approx \frac{|S|}{\eta}\left(\frac{b}{h}\right)^{1/2} t. \tag{3.22}$$

During this linear regime, a dynamic (receding) contact angle $\theta_d = \theta_Y/\sqrt{2}$ is formed at the three-phase contact line. In the subsequent stage (for hole radii approximately larger than the slip length b), the rim is fully established and grows in a self-similar manner. As discussed in section 3.2.1, this results in a characteristic $R \propto t^{2/3}$ growth law if large slip is present. That stage of self-similar growing rims is often called the 'mature' regime. These distinct regimes have been experimentally observed by Masson *et al* [108] and Damman *et al* [72]. Moreover, a dissipation dominated by slippage has been shown to be restricted to sufficiently small hole radii: if the rim has accumulated a very large amount of liquid (so that the height of the rim H_0 is much larger than the slip length b, i.e. $H_0 \gg b$), viscous dissipation dominates again. Consequently, this results in a transition to a linear growth law for the radius with respect to the dewetting time, i.e. $R \propto t$.

In this article, we mainly focus on dewetting phenomena in terms of growing holes or retracting straight fronts. Additionally, the subsequent regime influenced by the fingering instability has attracted the interest of researchers [109]. Therefore, facets such as the onset of the instability and the morphology of liquid profiles have also been shown to be sensitive to rheological properties of thin films and the hydrodynamic boundary condition at the solid/liquid interface [110–113].

3.3.2. 'Mature' holes. Recently, Fetzer *et al* experimentally studied the dewetting dynamics of 'mature' holes in thin PS films on two different types of hydrophobized surfaces. The aforementioned assumption of linear superposition of viscous dissipation and slippage (see section 3.2.3) was used to gain information about the slip contribution [86]. Hydrophobization was achieved by the preparation of a dense, self-assembled monolayer of silane molecules (silanization). In that case, two different silanes were utilized, octadecyltrichlorosilane (OTS) and dodecyltrichlorosilane (DTS). The slip length was shown to depend strongly on temperature (and, thereby, on the melt viscosity); in fact, the slip length decreased with increasing temperature. Furthermore, slippage was about one order of magnitude larger on DTS compared to OTS. The results are in accord with the results for the slip length gained by the analysis of the shape of rim profiles of the corresponding holes (see section 2.5.5). The molecular mechanisms of slippage are widely discussed and several models have been proposed with regard to different experimental conditions (shear rates, polymers, surfaces, etc). This will be discussed in section 3.4.

3.4. Molecular mechanisms of slippage

For small flow velocities, slip lengths lower than expected have been found (see e.g. [114]). This has been explained by the adsorption of polymer chains at the solid surface. These adsorbed chains are able to inhibit slippage due to entanglements with chains in the melt. At larger shear strains, disentanglement of adsorbed and melt chains occurs, the friction coefficient decreases rapidly and slippage is 'switched on' [115–118]. The authors interpret the results as follows: Strongly adsorbed chains stay at the solid/liquid interface followed by a coil-stretch transition of these tethered chains. Therefore, the interaction of anchored chains (which are stretched under high flow velocities) with the chains in the melt are reduced and slippage is enhanced. This has been experimentally observed by Migler *et al* [114] and Hervet *et al* [119]. Hence, the critical shear strain depends on the

molecular weight of chains attached to the surface and on their density [39]. This situation is also called 'stick–slip transition' and has, moreover, been reported for pressure-controlled capillary flow of polyethylene resins [120]. The authors find a characteristic molecular weight dependence of the slip length $b \propto M_w^{3.4}$, whereas the critical stress σ_c for the transition described before scales to $\sigma_c \propto M_w^{-0.5}$ [121]. Also, de-bonding of adsorbed chains might occur.

Molecular dynamics (MD) studies aiming to investigate the slip length in thin, short-chained polymer films subject to planar shear revealed a dynamic behavior of the slip length $b(\dot\gamma)$ upon the shear rate according to $b = b^*(1 - \dot\gamma/\dot\gamma_c)^{-1/2}$, where γ_c represents a critical shear rate [122]. Slippage strongly increases as $\dot\gamma/\dot\gamma_c \to 1$. This relation was also found for simple liquids. Additionally, the authors studied the border case $\dot\gamma \to 0$ and especially the molecular parameters affecting the slip length.

Moreover, a special situation has been discussed in the literature: a thin polymer film prepared on a surface decorated with end-grafted polymer chains of the same species. Due to entropic reasons, an interfacial tension between identical molecules occurs and dewetting can take place. This phenomenon is called autophobicity or autophobic dewetting [123, 124]. Reiter and Khanna observed that PDMS molecules slipped over grafted PDMS brushes. They found a slip length on the order of 10 μm for film thicknesses between 20 and 850 nm of the dewetting PDMS film (high M_w of 308 kg mol^{-1} in most cases). For lower grafting densities, slippage is reduced, indicating a deeper interpenetration of free melt chains [123].

3.5. Impact of viscoelasticity and stress relaxation

As already introduced in section 2.1.3 and, furthermore, theoretically described in section 2.5, viscoelasticity can be included in the description of thin film dynamics. In the case of thin film flow with strong slippage, we have already mentioned that the impact of viscoelasticity might not be distinguishable from slippage effects. Numerous experimental studies have been published by Reiter, Damman and co-workers describing the influence of viscoelastic effects on the flow dynamics of thin polymer films. These studies have been supported with theories by Raphaël and co-workers. In the following, a snapshot of recent results in chronological order is presented. It reflects the progress from simple to increasingly more sophisticated models and experiments. Some of the results, however, may have a tentative character, as mentioned in a very recent manuscript by Coppée *et al* (cf section 3.7).

3.5.1. Thin film rupture. Reiter and de Gennes [125] pointed out that the usual spin-casting preparation (based on fast solvent evaporation) of thin, long-chained polymer films may induce a cascade of distinct states. Annealing the samples to high temperatures for annealing times longer than the reptation time of the polymer (depending on M_w and the temperature T) might induce a complete healing of the preparation effects. Non-equilibrated conformational states and residual stresses have been shown to be capable of causing the rupture of thin films [126]. Therefore, the areal density of holes appearing at a certain temperature above T_g has been measured: after storage at elevated temperatures below T_g, an exponential reduction of the hole density can be observed. Vilmin and Raphaël were able to show that lateral stress reduces the critical value for surface fluctuations initiated by an anisotropic diffusion of polymer molecules to induce the formation of holes [127].

3.5.2. Stages of distinct dewetting dynamics—experimental results. Reiter and co-workers furthermore studied the temporal and spatial evolution of dewetting PS fronts on silicon wafers covered with a PDMS monolayer at times shorter than the relaxation (reptation) time τ_{rept} in equilibrated bulk samples [126]. At the beginning of their experiments, the dewetted distance and the rim width w increased in a logarithmic way with respect to the dewetting time t, consequently $V \propto t^{-1}$ is found. They correlated a maximum of the rim width w occurring at a distinct time t_1 (nearly independent on M_w and significantly shorter than τ_{rept}) of the experiment to a change in dewetting dynamics, namely $V \propto t^{-1/2}$ (i.e. $R \propto \sqrt{t}$).

Even before the aforementioned study, Damman *et al* compared the growth of a hole and the dynamics of a dewetting straight front [72]. Thus, the strong influence of the dewetting geometry on the dynamics of early stages became obvious. Moreover, the authors correlated their findings to the shape of the corresponding rim and clearly identified distinct dewetting stages: at the beginning of hole growth, capillary forces dominate the dynamics, and exponential growth is observed. In contrast to that, dewetting of a straight front at the beginning starts almost instantaneously at a high velocity and decreases as $V \propto t^{-1}$. As already observed by Redon *et al* [81], $V = \text{const}$ and $R \propto t$ due to viscous dissipation is found for growing holes. For both dewetting geometries, Damman *et al* find a maximum of the rim width w, which they interpret in terms of a transition of the shape of the rim from very asymmetric profiles towards more symmetric rims, while the volume still increases during dewetting. In the following dissipation-dominated regime, $V \propto t^{-1/3}$ and $R \propto t^{2/3}$ (slip boundary condition) or $V = \text{const}$ and $R \propto t$ (no-slip boundary condition) is found, depending on the boundary condition for the solid/liquid interface. Afterward, a constant dewetting velocity (until the 'mature rim' regime is reached and slippage dominates) is again obtained.

Recently, Damman and Reiter determined the strain γ from rim shapes of dewetting fronts, which can be written according to (2.3) as $\gamma = (S/h + \sigma_0)/G$, where σ_0 denotes residual stresses [128]. These values were one order of magnitude larger than for equilibrated PS films ($\gamma = S/(hG_{bulk})$) and increased with increasing M_w. Consequently, larger residual stresses σ_0 or smaller elastic moduli G can be responsible for this effect. Indeed, the elastic modulus of a thin film is supposed to be smaller than its bulk value, according to the fact that larger numbers for the entanglement length M_e (for larger M_w) are expected (see section 2.1.2). Additionally, instead of one transition time for both, two different transitions times t_w for the maximum of the rim width and t_v for the power law of the dewetting velocity (to $V \propto t^{-1/3}$) are

found for larger molecular weights. Time t_v is comparable to the reptation time t_{rept} (also for larger M_w). The authors interpret this as follows: after $t_v \sim t_{rept}$, the equilibrium entanglement conformation has been reached via interdiffusion and re-entangling of chains. Relaxation of stress, which is correlated to the rim shape transition and t_w, occurs at shorter times.

3.5.3. Stages of distinct dewetting dynamics—theoretical models. These observations have motivated a theoretical model by Vilmin and Raphaël [129] that takes viscoelastic properties of the liquid and slippage into account. The logarithmic increase of the dewetted distance with time can be explained if residual stress is regarded as an extra driving force for dewetting that has to be added to the capillary forces. Subsequent relaxation of the stress reduces this additional contribution. For times larger than the reptation time τ_{rept}, Vilmin and Raphaël predict a constant dewetting velocity and $V \propto t^{-1/3}$ as soon as the 'mature regime' is reached (and slippage becomes important). They consider a simple equation for a viscoelastic film, which includes one relaxation time τ_1 (and an elastic modulus G), but two distinct viscosities: η_0 is a short-time viscosity which describes the friction between monomers, and η_1 is the melt viscosity ($\eta_1 \ll \eta_0$) governed by disentanglements of polymer chains. Theoretically, three regimes of distinct time–response are expected: for $t < \tau_0 = \eta_0/G$, Newtonian flow accompanied by a small viscosity η_0. Afterward ($\tau_0 < t < \tau_1 = \eta_1/G$), the elastic modulus governs the dynamics. For longer times, i.e. $t > \tau_1$, Newtonian flow is again obtained, but with a much larger viscosity η_1. During the first and the last regime, asymmetric rims and constant velocities are predicted (the latter velocity, of course, is much smaller than the initial velocity). The intermediate regime, governed by viscoelastic behavior, is expected to show $V \propto t^{-1/2}$, according to the fact that the width of the rim w will increase proportionally to the dewetted distance D, i.e. $w \propto D$ (in contrast to the square-root dependence in cases of viscous flow). Including residual stresses into their model, Vilmin and Raphaël obtained the aforementioned experimentally observed $V \propto t^{-1}$ law instead of $V \propto t^{-1/2}$. Recently, Yang *et al* experimentally quantified the molecular recoiling force stemming from non-equilibrium chain conformations. They obtained values that are at least comparable to (or even larger than) the dispersive driving forces [130].

3.5.4. Further remarks. Concerning studies and models including viscoelastic effects, one has to bear in mind that stress relaxation dynamics and relaxation times in thin films have been shown to be different from bulk polymer reptation values. As mentioned in section 2.1.2 and indicated by the characteristic relaxation times τ_1 of elastic constraints being significantly shorter than bulk values, the entanglement length has been shown to be significantly higher in the case of thin films.

Recently, Reiter and co-workers extended their studies with regard to viscoelastic dewetting on soft, deformable substrates [100]. The essential result was that transient residual stresses can cause large elastic deformations in the substrate which almost stop dewetting for times shorter than the relaxation time τ_{rept} of the polymer film. For times longer than τ_{rept}, the elastic behavior and the elastic trench in the deformable substrate vanishes.

Vilmin and Raphaël applied their model for viscoelastic liquids and residual stresses to the hole growth geometry [131] with regard to the early stage (exponential growth for Newtonian liquids). They discovered a very rapid opening regime followed by slow exponential growth of the radius of the holes.

3.6. Non-linear friction

With regard to energy dissipation at the solid/liquid interface, linear friction has been exclusively considered up to now. As described in section 3.4, often not only have smooth and passive (non-adsorbing) surfaces been experimentally considered, but grafted or adsorbed polymer layers are also used as a support for dewetting experiments. These systems motivate the theoretical treatment of non-linear friction, as described in section 3.6.1.

3.6.1. Theoretical model. To cover non-linear friction, Vilmin and Raphaël introduced a friction force per unit area that is linear below a certain transition velocity v_r and non-linear above [131]:

$$F_s = \xi v_r (v/v_r)^{1-r}, \qquad v > v_r, \tag{3.23}$$

where r denotes a *friction exponent*. Consequently, the effective (velocity-dependent) friction coefficient ξ_{eff} can be written in terms of

$$\xi_{eff}(v) = \xi (v_r/v)^r \tag{3.24}$$

and a velocity-dependent slip length $b(v)$ can be defined as

$$b(v) = \eta/\xi_{eff}(v). \tag{3.25}$$

An increasing velocity leads to a decreasing friction coefficient and to pronounced slippage. The friction at the solid/liquid interface influences the power law of the velocity decrease. Assuming non-linear friction in the intermediate regime (which is governed by the viscoelastic behavior) gives (according to $w \propto D$) $V \propto t^{-1/(2-r)}$. Including residual stress σ_0 to this model leads to a formula for the maximum width of the rim (depending on r and σ_0). Experimentally, values for r between 0 (for low M_w) and 1 (for large M_w) have been found [128]. The dependence of the non-linearity of friction upon molecular weight M_w could be explained by the influence of chain length on slippage (see (3.12)).

3.6.2. Variation of substrate properties. Hamieh *et al* focused on the frictional behavior of dewetting viscoelastic PS films on PDMS-coated (irreversibly adsorbed) silicon wafers [132]. Thereby, thickness (via the PDMS chain length) and preparation of the PDMS support (via the annealing temperature) were varied. In summary, the observations are consistent with the aforementioned (section 3.5) experiments

by Reiter, showing a characteristic time t_1 for the change in dewetting dynamics and rim shape (from highly asymmetric towards a more symmetric equilibrated shape). Again, this transition is interpreted by the Laplace pressure that overcomes elastic effects. Probing the maximum rim width enables the authors to identify the impact of the friction coefficient or the friction exponent r: if they prepare thicker PDMS layers, the result is a larger maximum rim width. This result can be explained in terms of a small increase of r. Consequently, the velocity-dependent slip length $b(v)$ increases (see (3.25)): thicker PDMS layers lead to more slippage. Concerning the characteristic time for stress relaxation t_1, no significant influence of the preparation procedure (annealing temperature of the PDMS coating) and thickness of the PDMS layer have been found.

3.7. Temporal evolution of the slip length

Most of the aforementioned dewetting experiments of thin (viscoelastic) PS films are based on supports consisting of a PDMS layer prepared onto a Si wafer. These PDMS surfaces, which were assumed to be impenetrable by PS chains, proved to be less ideal. Recently, the aforementioned fast decay of the dewetting velocity and the maximum of the rim width upon dewetting time (ascribed to relaxation of residual stresses, see section 3.5) has also been observed in the case of low molecular weight PS [133]. Furthermore, neutron reflectometry experiments revealed an interdiffusion of polymer chains at the PS-PDMS interface below the PS bulk glass transition temperature. The dewetting velocity accelerated as the brush thickness is increased. In view of energy dissipation due to brush deformation (pronounced by increasing thickness), this is in contradiction to the slower dewetting velocities expected in that case.

Ziebert and Raphaël recently investigated the temporal evolution of the energy balance (viscous dissipation and sliding friction) of thin film dewetting by numerical treatment, especially concerning non-linear friction [134]. They point out that both mechanisms have different time dependences and propose that simple scaling arguments, such as the mass conservation $w \propto D$, should be revisited. In cases of non-linear friction, viscous dissipation is even more important than sliding friction for times larger than τ_1, whereas, for linear friction, both mechanisms are almost equally important. The stage of 'mature' rims afterward is again dominated by friction at the solid/liquid interface. Using scaling arguments and numerical solutions of the thin film model for viscoelastic liquids [129], they further showed that the aforementioned dewetting characteristics (fast decay of the dewetting velocity, maximum of the rim width in course of dewetting time) can be explained by the temporal decrease of the slip length during the experiment instead of stress relaxation [135]. Therefore, roughening of the PS-PDMS interface (as detected by neutron reflectometry) or potentially an attachment of very few PS chains to the silicon substrate might also be responsible if very low PDMS grafting densities are prepared.

The attachment of melt chains to the substrate has been recently considered by Reiter *et al* [136]. They pointed out that the driving force is reduced by a certain pull-out force for molecules attached to the surface as they get stretched while resisting to be pulled out. Consequently, this force (per unit length of the contact line) can be written in terms of $F_p = \nu L f^*$, where ν represents the number of surface-connected molecules, L the length according to the stretching and f^* the pull-out force per chain.

4. Conclusions and outlook

To conclude, dewetting experiments can be regarded as a very powerful tool to probe rheological thin film properties and frictional mechanisms. The validity of the no-slip boundary condition at the solid/liquid interface, for a long period of time accepted as a standard approach in fluid dynamics, fails. Even for Newtonian liquids, such as polymers below their critical length for entanglements, substantial amounts of slippage have been found. For larger molecular weights, slippage can be even more pronounced if chain entanglements come into play.

We have reviewed in this article theories and experiments characterizing the statics and dynamics in thin liquid polymer films, focusing on energy dissipation mechanisms occurring during dewetting. Experiments are relatively easy to perform, since usually no very low or very high temperatures are needed, neither are high-speed cameras necessary. However, careful preparation, preferably in a clean-room environment, of thin films is inevitable. Concerning the experimental data, diligent interpretation and consideration of all relevant parameters are of essential importance: molecular weight, film thickness (also with regard to the molecular dimensions of a polymer coil in the respective melt), dewetting temperature, melt viscosity, dewetting velocity and capillary number, residual stresses, relaxation times and aging time represent parameters that are sometimes coupled and not easy to disentangle. Their unique impact on the friction coefficient or the slip length on a specific, ideally non-adsorbing and non-penetrable substrate (to reduce the number of parameters of the system) is not always easy to identify. In particular, the specific stage of dewetting (early or mature stage) and the dewetting geometry (holes or straight fronts) represent further facets and playgrounds for experimentalists and theoreticians that, under careful consideration, enable the gaining of insight into rheological or frictional mechanisms. The dynamics and the morphology of the fingering instability can provide additional access to the solid/liquid boundary condition and the rheology.

Obtaining a deeper understanding of the molecular mechanisms at the solid/liquid interface is one of the main tasks in micro- and nanofluidics. In this context, we would like to highlight two essential questions and possible pathways to answer them.

(i) The liquid: what is the impact of the polydispersity of the liquid on dewetting? Dewetting studies of polymer melts by adding a second chemical component have been shown to influence slippage [137]. However, also the driving force is changed due to the difference in chemical composition for different species. To overcome this problem, the influence of chain length distribution on

dewetting can be probed by studying polymer mixtures instead of monodisperse polymer melts [138]. With regard to a theoretical approach to this question, dissipative particle dynamics (DPD) simulations enable the location of energy loss in the rim and reveal interesting results in the case of two immiscible fluids of different viscosities: in cases of a low-viscosity layer at the solid/liquid interface, faster dewetting dynamics are found that are attributed to a lubrication effect, i.e. the sliding of the upper high-viscosity layer [139]. Finally, these aspects lead to the fundamental discussion of whether 'apparent' slip, possibly induced by the formation of a short-chained layer of low viscosity, is present. In cases of entangled polymer melts, we very recently found evidence for a reduced entanglement density in the vicinity of the solid/liquid interface, which strongly affects the slippage properties of thin polymer films [140].

(ii) The substrate: what is the impact of the molecular structure of the substrate? As indicated before, the set of parameters concerning the topographical and/or chemical structure of the support is large. Besides parameters such as surface roughness and surface energy, experiments can be performed on substrates, e.g. decorated with an amorphous coating, a self-assembled monolayer or even grafted polymer brushes of the same or different species. Scattering techniques (using neutrons or x-rays) provide access to the solid/liquid interface, complementing dewetting experiments and confirming proposed mechanisms of slippage. Simulations based on molecular dynamics (MD) of near-surface flows can help to compare experimental results from dewetting studies to molecular parameters, easily tunable in theoretical models, and structural changes [141, 142]. Moreover, the evolution of coarse-grained polymer brush/melt interfaces under flow has also been identified as a potential application of MD studies z [143, 144]. In the end, all these facets help to obtain a universal picture of sliding friction which can potentially lead to surfaces precisely tailored to special microfluidic applications.

Acknowledgments

The authors acknowledge financial support from the German Science Foundation (DFG) under grant JA905/3 within the priority program 1165 *'Micro- and nanofluidics'*.

References

[1] Squires T M and Quake S R 2005 Microfluidics: fluid physics at the nanoliter scale *Rev. Mod. Phys.* **77** 977
[2] Thorsen T, Maerkl S J and Quake S R 2002 Microfluidic large-scale integration *Science* **298** 580
[3] Leslie D C, Easley C J, Seker E, Karlinsey J M, Utz M, Begley M R and Landers J P 2009 Frequency-specific flow control in microfluidic circuits with passive elastomeric features *Nat. Phys.* **5** 231
[4] Bear J 1972 *Dynamics of Fluids in Porous Media* (New York: Elsevier)
[5] Vrij A 1966 Possible mechanism for the spontaneous rupture of thin, free liquid films *Discuss. Faraday Soc.* **42** 14
[6] Herminghaus S, Jacobs K, Mecke K, Bischof J, Fery A, Ibn-Elhaj M and Schlagowski S 1998 Spinodal dewetting in liquid crystal and liquid metal films *Science* **282** 916
[7] Seemann R, Herminghaus S and Jacobs K 2001 Dewetting patterns and molecular forces: a reconciliation *Phys. Rev. Lett.* **86** 5534
[8] Jacobs K, Seemann R and Herminghaus S 2008 Stability and dewetting of thin liquid films *Polymer Thin Films* ed O K C Tsui and T P Russell (Singapore: World Scientific)
[9] Seemann R, Herminghaus S and Jacobs K 2001 Gaining control of pattern formation of dewetting liquid films *J. Phys.: Condens. Matter* **13** 4925
[10] Jacobs K, Seemann R and Mecke K 2000 Dynamics of structure formation in thin films: a special spatial analysis *Statistical Physics and Spatial Statistics* (*Springer Lecture Notes in Physics*) ed D Stoyan and K Mecke (Heidelberg: Springer)
[11] Craster R V and Matar O K 2009 Dynamics and stability of thin liquid films *Rev. Mod. Phys.* **81** 1131
[12] Rubinstein M and Colby R H 2003 *Polymer Physics* (New York: Oxford University Press)
[13] Jones R A L and Richards R W 1999 *Polymers at Surfaces and Interfaces* (Cambridge: Cambridge University Press)
[14] De Gennes P G 1971 Reptation of a polymer chain in the presence of fixed obstacles *J. Chem. Phys.* **55** 572
[15] Keddie J L, Jones R A L and Cory R A 1994 Size-dependent depression of the glass transition temperature in polymer films *Europhys. Lett.* **27** 59
[16] Mattsson J, Forrest J A and Börgesson L 2000 Quantifying glass transition behavior in ultrathin free-standing polymer films *Phys. Rev.* E **62** 5187
[17] Dalnoki-Veress K, Forrest J A, de Gennes P-G and Dutcher J R 2000 Glass transition reductions in thin freely-standing polymer films: a scaling analysis of chain confinement effects *J. Physique* **10** 221
[18] Herminghaus S, Jacobs K and Seemann R 2001 The glass transition of thin polymer films: some questions, and a possible answer *Eur. Phys. J.* E **5** 531
[19] Keddie J L and Jones R A L 1995 Glass transition behavior in ultrathin polystyrene films *J. Isr. Chem. Soc.* **35** 21
[20] Fryer D S, Peters R D, Kim E J, Tomaszewski J E, De Pablo J J and Nealey P F 2001 Dependence of the glass transition temperature of polymer films on interfacial energy and thickness *Macromolecules* **34** 5627
[21] Herminghaus S, Jacobs K and Seemann R 2003 Viscoelastic dynamics of polymer thin films and surfaces *Eur. Phys. J.* E **12** 101
[22] Kawana S and Jones R A L 2001 Character of the glass transition in thin supported polymer films *Phys. Rev.* E **63** 021501
[23] Herminghaus S, Seemann R and Landfester K 2004 Polymer surface melting mediated by capillary waves *Phys. Rev. Lett.* **93** 017801
[24] Seemann R, Jacobs K, Landfester K and Herminghaus S 2006 Freezing of polymer thin films and surfaces: the small molecular weight puzzle *J. polym. Sci.* B **44** 2968
[25] Si L, Massa M V, Dalnoki-Veress K, Brown H R and Jones R A L 2005 Chain entanglement in thin freestanding polymer films *Phys. Rev. Lett.* **94** 127801
[26] Rauscher M, Münch A, Wagner B and Blossey R 2005 A thin-film equation for viscoelastic liquids of Jeffreys type *Eur. Phys. J.* E **17** 373
[27] Blossey R, Münch A, Rauscher M and Wagner B 2006 Slip versus viscoelasticity in dewetting thin films *Eur. Phys. J.* E **20** 267
[28] Münch A, Wagner B, Rauscher M and Blossey R 2006 A thin-film model for corotational Jeffreys fluids under strong slip *Eur. Phys. J.* E **20** 365
[29] Te Nijenhuis K, McKinley G H, Spiegelberg S, Barnes H A, Aksel N, Heymann L and Odell J A 2007 Non-Newtonian flows *Springer Handbook of Experimental Fluid Mechanics* ed C Tropea, A L Yarin and J F Foss (Berlin: Springer)

[30] Münch A, Wagner B A and Witelski T P 2005 Lubrication models with small to large slip lengths *J. Eng. Math.* **53** 359

[31] Navier C L M H 1823 Mémoire sur les lois du mouvement des fluids *Mem. Acad. Sci. Inst. Fr.* **6** 389
Navier C L M H 1823 Mémoire sur les lois du mouvement des fluids *Mem. Acad. Sci. Inst. Fr.* **6** 432

[32] Lauga E, Brenner M P and Stone H A 2007 Microfluidics: the no-slip boundary condition *Springer Handbook of Experimental Fluid Mechanics* ed C Tropea, A L Yarin and J F Foss (Berlin: Springer)

[33] Neto C, Evans D R, Bonaccurso E, Butt H-J and Craig V S J 2005 Boundary slip in Newtonian liquids: a review of experimental studies *Rep. Prog. Phys.* **68** 2859

[34] Bocquet L and Barrat J-L 2007 Flow boundary conditions from nano-to micro-scales *Soft Matter* **3** 685

[35] Joly L, Ybert C and Bocquet L 2006 Probing the nanohydrodynamics at liquid/solid interfaces using thermal motion *Phys. Rev. Lett.* **96** 046101

[36] Barrat J-L and Bocquet L 1999 Large slip effect at a nonwetting fluid-solid interface *Phys. Rev. Lett.* **82** 4671

[37] Pit R, Hervet H and Léger L 2000 Direct experimental evidence of slip in hexadecane: solid interfaces *Phys. Rev. Lett.* **85** 980

[38] Cottin-Bizonne C, Jurine S, Baudry J, Crassous J, Restagno F and Charlaix E 2002 Nanorheology: an investigation of the boundary condition at hydrophobic and hydrophilic interfaces *Eur. Phys. J.* E **9** 47

[39] Leger L 2003 Friction mechanisms and interfacial slip at fluid–solid interfaces *J. Phys.: Condens. Matter* **15** S19

[40] Zhu Y and Granick S 2002 Limits of the hydrodynamic no-slip boundary condition *Phys. Rev. Lett.* **88** 106102

[41] Schmatko T, Hervet H and Léger L 2006 Effect of nano-scale roughness on slip at the wall of simple fluids *Langmuir* **22** 6843

[42] Kunert C and Harting J 2007 Roughness induced boundary slip in microchannel flows *Phys. Rev. Lett.* **99** 176001

[43] Cottin-Bizonne C, Barrat J-L, Bocquet L and Charlaix E 2003 Low-friction flows of liquid at nanopatterned interfaces *Nat. Mater.* **2** 237

[44] Priezjev N V and Troian S M 2006 Influence of periodic wall roughness on the slip behaviour at liquid/solid interfaces: molecular-scale simulations versus continuum predictions *J. Fluid Mech.* **554** 25

[45] Joseph P, Cottin-Bizonne C, Benoît J-M, Ybert C, Journet C, Tabeling P and Bocquet L 2006 Slippage of water past superhydrophobic carbon nanotube forests in microchannels *Phys. Rev. lett.* **97** 156104

[46] Ybert C, Barentin C, Cottin-Bizonne C, Joseph P and Bocquet L 2007 Achieving large slip with superhydrophobic surfaces: scaling laws for generic geometries *Phys. Fluids* **19** 123601

[47] Steinberger A, Cottin-Bizonne C, Kleimann P and Charlaix E 2007 High friction on a bubble mattress *Nat. Mater.* **6** 665

[48] Schmatko T, Hervet H and Léger L 2005 Friction and slip at simple fluid/solid interfaces: the roles of the molecular shape and the solid/liquid interaction *Phys. Rev. Lett.* **94** 244501

[49] Priezjev N V, Darhuber A A and Troian S M 2005 Slip behavior in liquid films on surfaces of patterned wettability: comparison between continuum and molecular dynamics simulations *Phys. Rev.* E **71** 041608

[50] Heidenreich S, Ilg P and Hess S 2007 Boundary conditions for fluids with internal orientational degrees of freedom: apparent velocity slip associated with the molecular alignment *Phys. Rev.* E **75** 066302

[51] Cho J-H J, Law B M and Rieutord F 2004 Dipole-dependent slip of Newtonian liquids at smooth solid hydrophobic surfaces *Phys. Rev. Lett.* **92** 166102

[52] De Gennes P G 2002 On fluid/wall slippage *Langmuir* **18** 3413

[53] Huang D M, Sendner C, Horinek D, Netz R R and Bocquet L 2008 Water slippage versus contact angle: a quasiuniversial relationship *Phys. Rev. Lett.* **101** 226101

[54] Steitz R, Gutberlet T, Hauss T, Klösgen B, Krastev R, Schemmel S, Simonsen A C and Findenegg G H 2003 Nanobubbles and their precursor layer at the interface of water against a hydrophobic substrate *Langmuir* **19** 2409

[55] Doshi D A, Watkins E B, Israelachvili J N and Majewski J 2005 Reduced water density at hydrophobic surfaces: effect of dissolved gases *Proc. Natl Acad. Sci.* **102** 9458

[56] Mezger M, Reichert H, Schröder S, Okasinski J, Schröder H, Dosch H, Palms D, Ralston J and Honkimäki V 2006 High-resolution *in situ* x-ray study of the hydrophobic gap at the water-octadecyl-trichlorosilane interface *Proc. Natl Acad. Sci.* **103** 18401

[57] Maccarini M, Steitz R, Himmelhaus M, Fick J, Tatur S, Wolff M, Grunze M, Janeček J and Netz R R 2007 Density depletion at solid–liquid interfaces: a neutron reflectivity study *Langmuir* **23** 598

[58] Tyrrell J W G and Attard P 2001 Images of nanobubbles on hydrophobic surfaces and their interactions *Phys. Rev. Lett.* **87** 176104

[59] Tretheway D C and Meinhart C D 2004 A generating mechanism for apparent fluid slip in hydrophobic microchannels *Phys. Fluids* **16** 1509

[60] Poynor A, Hong L, Robinson I K, Granick S, Zhang Z and Fenter P A 2006 How water meets a hydrophobic surface *Phys. Rev. Lett.* **97** 266101

[61] Hendy S C and Lund N J 2009 Effective slip length for flows over surfaces with nanobubbles: the effect of finite slip *J. Phys.: Condens. Matter* **21** 144202

[62] Oron A, Davis S H and Bankoff S G 1997 Long-scale evolution of thin liquid films *Rev. Mod. Phys.* **69** 931

[63] Kargupta K, Sharma A and Khanna R 2004 Instability, dynamics, and morphology of thin slipping films *Langmuir* **20** 244

[64] Fetzer R, Münch A, Wagner B, Rauscher M and Jacobs K 2007 Quantifying hydrodynamic slip: a comprehensive analysis of dewetting profiles *Langmuir* **23** 10559

[65] Blossey R 2008 Thin film rupture and polymer flow *Phys. Chem. Chem. Phys.* **10** 5177

[66] Israelachvili J 1992 *Intermolecular and Surface Forces* 2nd edn (New York: Academic)

[67] Becker J, Grün G, Seemann R, Mantz H, Jacobs K, Mecke K R and Blossey R 2003 Complex dewetting scenarios captured by thin-film models *Nat. Mater.* **2** 59

[68] Rauscher M, Blossey R, Münch A and Wagner B 2008 Spinodal dewetting of thin films with large interfacial slip: implications from the dispersion relation *Langmuir* **24** 12290

[69] Fetzer R, Rauscher M, Seemann R, Jacobs K and Mecke K 2007 Thermal noise influences fluid flow in thin films during spinodal dewetting *Phys. Rev. Lett.* **99** 114503

[70] Seemann R, Herminghaus S and Jacobs K 2001 Shape of a liquid front upon dewetting *Phys. Rev. Lett.* **87** 196101

[71] Reiter G 2001 Dewetting of highly elastic thin polymer films *Phys. Rev. Lett.* **87** 186101

[72] Damman P, Baudelet N and Reiter G 2003 Dewetting near the glass transition: transition from a capillary force dominated to a dissipation dominated regime *Phys. Rev. Lett.* **91** 216101

[73] Neto C, Jacobs K, Seemann R, Blossey R, Becker J and Grün G 2003 Correlated dewetting patterns in thin polystyrene films *J. Phys.: Condens. Matter* **15** 421

[74] Neto C, Jacobs K, Seemann R, Blossey R, Becker J and Grün G 2003 Satellite hole formation during dewetting: experiment and simulation *J. Phys.: Condens. Matter* **15** 3355

[75] Fetzer R, Jacobs K, Münch A, Wagner B and Witelski T P 2005 New slip regimes and the shape of dewetting thin liquid films *Phys. Rev. Lett.* **95** 127801

[76] Fetzer R, Rauscher M, Münch A, Wagner B A and Jacobs K 2006 Slip-controlled thin film dynamics *Europhys. Lett.* **75** 638

[77] Bäumchen O, Fetzer R, Münch A, Wagner B and Jacobs K 2009 Comprehensive analysis of dewetting profiles to quantify hydrodynamic slip *IUTAM Symp. on Adv. in Micro- and Nanofluidics* ed M Ellero, X Hu, J Fröhlich and N Adams (Berlin: Springer)

[78] De Gennes P G 1985 Wetting: statics and dynamics *Rev. Mod. Phys.* **57** 827

[79] Frumkin A N 1938 On the wetting phenomena and attachment of bubbles I *J. Phys. Chem. USSR* **12** 337

[80] Brochard-Wyart F, De Gennes P-G, Hervet H and Redon C 1994 Wetting and slippage of polymer melts on semi-ideal surfaces *Langmuir* **10** 1566

[81] Redon C, Brochard-Wyart F and Rondelez F 1991 Dynamics of dewetting *Phys. Rev. Lett.* **66** 715

[82] Redon C, Brzoska J B and Brochard-Wyart F 1994 Dewetting and slippage of microscopic polymer films *Macromolecules* **27** 468

[83] De Gennes P G 1979 Ecoulements viscométriques de polymères enchevêtrés *C. R. Acad. Sci.* B **288** 219

[84] Münch A 2005 Dewetting rates of thin liquid films *J. Phys.: Condens. Matter* **17** S309

[85] Jacobs K, Seemann R, Schatz G and Herminghaus S 1998 Growth of holes in liquid films with partial slippage *Langmuir* **14** 4961

[86] Fetzer R and Jacobs K 2007 Slippage of newtonian liquids: influence on the dynamics of dewetting thin films *Langmuir* **23** 11617

[87] Bäumchen O, Jacobs K and Fetzer R 2008 Probing slippage and flow dynamics of thin dewetting polymer films *Proc. Eur. Conf. on Microfluidics ((Bologna, Dec., 2008))*

[88] Blake T D and Haynes J M 1969 Kinetics of liquid/liquid displacement *J. Colloid Interface Sci.* **30** 421

[89] De Ruijter M J, Blake T D and De Coninck J 1999 Dynamic wetting studied by molecular modeling simulations of droplet spreading *Langmuir* **15** 7836

[90] Blake T D and De Coninck J 2002 The influence of solid/liquid interactions on dynamic wetting *J. Adv. Colloid Interface Sci.* **96** 21

[91] Voué M, Rioboo R, Adao M H, Conti J, Bondar A I, Ivanov D A, Blake T D and De Coninck J 2007 Contact-line friction of liquid drops on self-assembled monolayers: chain-length effects *Langmuir* **23** 4695

[92] Barrena E, Kopta S, Ogletree D F, Charych D H and Salmeron M 1999 Relationship between friction and molecular structure: alkylsilane lubricant films under pressure *Phys. Rev. Lett.* **82** 2880

[93] Shanahan M E R and Carré A 1994 Anomalous spreading of liquid drops on an elastomeric surface *Langmuir* **10** 1647

[94] Shanahan M E R and Carré A 1995 Viscoelastic dissipation in wetting and adhesion phenomena *Langmuir* **11** 1396

[95] Carré A and Shanahan M E R 1995 Influence of the 'wetting ridge' in dry patch formation *Langmuir* **11** 3572

[96] Carré A, Gastel J-C and Shanahan M E R 1996 viscoelastic effects in the spreading of liquids *Nature* **379** 432

[97] Shanahan M E R and Carré A 2002 Spreading and dynamics of liquid drops involving nanometric deformations on soft substrates *Colloids Surf.* A **206** 115

[98] Long D, Ajdari A and Leibler L 1996 Static and dynamic wetting properties of thin rubber films *Langmuir* **12** 5221

[99] Long D, Ajdari A and Leibler L 1996 How do grafted polymer layers alter the dynamics of wetting *Langmuir* **12** 1675

[100] Al Akhrass S, Reiter G, Hou S Y, Yang M H, Chang Y L, Chang F C, Wang C F and Yang A C-M 2008 Viscoelastic thin polymer films under transient residual stresses: two-stage dewetting on soft substrates *Phys. Rev. Lett.* **100** 178301

[101] Ruckenstein E and Jain R K 1974 Spontaneous rupture of thin liquid films *J. Chem. Soc. Faraday Trans.* II **132**

[102] Brochard-Wyart F, Di Meglio J-M and Quéré D 1987 Dewetting *C. R. Acad. Sci. Paris* II **304** 553

[103] Sharma A and Ruckenstein E 1989 Dewetting of solids by the formation of holes in macroscopic liquid films *J. Colloid Interface Sci.* **133** 358

[104] Brochard-Wyart F and Daillant J 1990 Drying of solids wetted by thin liquid films *Can. J. Phys.* **68** 1084

[105] Brochard-Wyart F, Redon C and Skykes C 1992 Dewetting of ultrathin liquid films *C.R. Acad. Sci. Paris* II **314** 19

[106] Reiter G 1992 Dewetting of thin polymer films *Phys. Rev. Lett.* **68** 75

[107] Brochard-Wyart F, Debregeas G, Fondecave R and Martin P 1997 Dewetting of supported viscoelastic polymer films: birth of rims *Macromolecules* **30** 1211

[108] Masson J-L and Green P F 2002 Hole formation in thin polymer films: a two-stage process *Phys. Rev. Lett.* **88** 205504

[109] Brochard-Wyart F and Redon C 1992 Dynamics of rim instabilities *Langmuir* **8** 2324

[110] Reiter G and Sharma A 2001 Auto-optimization of dewetting rates by rim instabilities in slipping polymer films *Phys. Rev. Lett.* **87** 166103

[111] Münch A and Wagner B 2005 Contact-line instability of dewetting thin films *Physica* D **209** 178

[112] Gabriele S, Sclavons S, Reiter G and Damman P 2006 Disentanglement time of polymers determines the onset of rim instabilities in dewetting *Phys. Rev. Lett.* **96** 156105

[113] King J R, Münch A and Wagner B 2009 Linear stability analysis of a sharp-interface model for dewetting thin films *J. Eng. Math.* **63** 177

[114] Migler K B, Hervet H and Leger L 1993 Slip transition of a polymer melt under shear stress *Phys. Rev. Lett.* **70** 287

[115] Brochard F and de Gennes P G 1992 Shear-dependent slippage at a polymer/solid interface *Langmuir* **8** 3033

[116] Ajdari A, Brochard-Wyart F, De Gennes P-G, Leibler L, Viovy J-L and Rubinstein M 1994 Slippage of an entangled polymer melt on a grafted surface *Physica* A **204** 17

[117] Gay C 1999 New concepts for the slippage of an entangled polymer melt at a grafted solid interface *Eur. Phys. J.* B **7** 251

[118] Tchesnokov M A, Molenaar J, Slot J J M and Stepanyan R 2005 A molecular model for cohesive slip at polymer melt/solid interfaces *J. Chem. Phys.* **122** 214711

[119] Hervet H and Leger L 2003 Flow with slip at the wall: from simple to complex fluids *C. R. Physique* **4** 241

[120] Drda P P and Wang S-Q 1995 Stick–slip transition at polymer melt/solid interfaces *Phys. Rev. Lett.* **75** 2698

[121] Wang S-Q and Drda P A 1996 Stick-slip transition in capillary flow of polyethylene. 2. Molecular-weight dependence and low-temperature anomaly *Macromolecules* **29** 4115

[122] Priezjev N V and Troian S M 2004 Molecular origin and dynamic behavior of slip in sheared polymer films *Phys. Rev. Lett.* **92** 018302

[123] Reiter G and Khanna R 2000 Kinetics of autophobic dewetting of polymer films *Langmuir* **16** 6351

[124] Reiter G and Khanna R 2000 Negative excess interfacial entropy between free and end-grafted chemically identical polymers *Phys. Rev. Lett.* **85** 5599

[125] Reiter G and De Gennes P-G 2001 Spin-cast, thin, glassy polymer films: highly metastable forms of matter *Eur. Phys. J.* E **6** 25

[126] Reiter G, Hamieh M, Damman P, Sclavons S, Gabriele S, Vilmin T and Raphaël E 2005 Residual stresses in thin polymer films cause rupture and dominate early stages of dewetting *Nat. Mater.* **4** 754
[127] Vilmin T and Raphaël E 2006 Dynamic instability of thin viscoelastic films under lateral stress *Phys. Rev. Lett.* **97** 036105
[128] Damman P, Gabriele S, Coppée S, Desprez S, Villers D, Vilmin T, Raphaël E, Hamieh M, Al Akhrass S and Reiter G 2007 Relaxation of residual stress and reentanglement of polymers in spin-coated films *Phys. Rev. Lett.* **99** 036101
[129] Vilmin T and Raphaël E 2005 Dewetting of thin viscoelastic polymer films on slippery substrates *Europhys. Lett.* **72** 781
[130] Yang M H, Hou S Y, Chang Y L and Yang A C-M 2006 Molecular recoiling in polymer thin film dewetting *Phys. Rev. Lett.* **96** 066105
[131] Vilmin T and Raphaë l 2006 Dewetting of thin polymer films *Eur. Phys. J.* E **21** 161
[132] Hamieh M, Al Akhrass S, Hamieh T, Damman P, Gabriele S, Vilmin T, Raphaël E and Reiter G 2007 Influence of substrate properties on the dewetting dynamics of viscoelastic polymer films *J. Adhes.* **83** 367
[133] Coppée S, Gabriele S, Jonas A M, Jestin J and Damman P 2009 Influence of chain interdiffusion between immiscible polymers on dewetting dynamics arXiv:0904.1675v1
[134] Ziebert F and Raphaël E 2009 Dewetting dynamics of stressed viscoelastic thin polymer films *Phys. Rev.* E **79** 031605
[135] Ziebert F and Raphaël E 2009 Dewetting of thin polymer films: influence of interface evolution *Europhys. Lett.* **86** 46001
[136] Reiter G, Al Akhrass S, Hamieh M, Damman P, Gabriele S, Vilmin T and Raphaël E 2009 Dewetting as an investigative tool for studying properties of thin polymer films *Eur. Phys. J.* **166** 165 Special Topics
[137] Besancon B M and Green P F 2007 Dewetting dynamics in miscible polymer–polymer thin films mixtures *J. Chem. Phys.* **126** 224903
[138] Fetzer R 2006 *Einfluss von Grenzflächen auf die Fluidik dünner Polymerfilme* (Berlin: Logos)
[139] Merabia S and Avalos J B 2008 Dewetting of a stratified two-component liquid film on a solid substrate *Phys. Rev. Lett.* **101** 208304
[140] Bäumchen O, Fetzer R and Jacobs K 2009 Reduced interfacial entanglement density affects the boundary conditions of polymer flow *Phys. Rev. Lett.* at press
[141] Servantie J and Müller M 2008 Temperature dependence of the slip length in polymer melts at attractive surfaces *Phys. Rev. Lett.* **101** 026101
[142] Müller M, Pastorino C and Servantie J 2008 Flow, slippage and a hydrodynamic boundary condition of polymers at surfaces *J. Phys.: Condens. Matter* **20** 494225
[143] Pastorino C, Binder K, Kreer T and Müller M 2006 Static and dynamic properties of the interface between a polymer brush and a melt of identical chains *J. Chem. Phys.* **124** 064902
[144] Pastorino C, Binder K and Müller M 2009 Coarse-grained description of a brush/melt interface in equilibrium and under flow *Macromolecules* **42** 401